Provided for non-commercial research and educational use only.
Not for reproduction or distribution or commercial use.

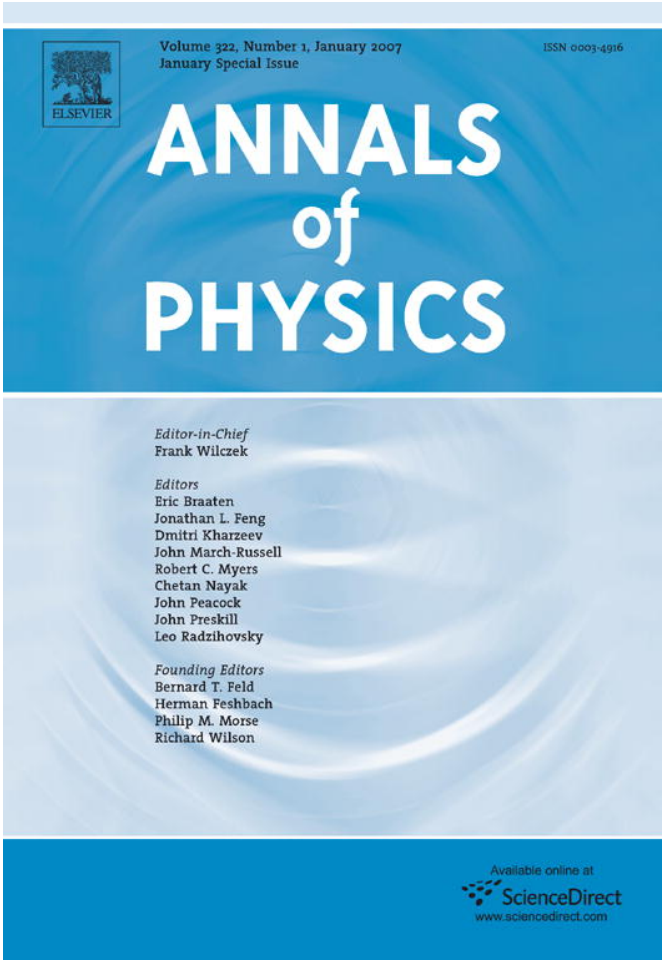

This article was originally published in a journal published by Elsevier, and the attached copy is provided by Elsevier for the author's benefit and for the benefit of the author's institution, for non-commercial research and educational use including without limitation use in instruction at your institution, sending it to specific colleagues that you know, and providing a copy to your institution's administrator.

All other uses, reproduction and distribution, including without limitation commercial reprints, selling or licensing copies or access, or posting on open internet sites, your personal or institution's website or repository, are prohibited. For exceptions, permission may be sought for such use through Elsevier's permissions site at:

http://www.elsevier.com/locate/permissionusematerial

Available online at www.sciencedirect.com
ScienceDirect
Annals of Physics 322 (2007) 164–200
ANNALS of PHYSICS
www.elsevier.com/locate/aop

Hamiltonian systems with detuned 1:1:2 resonance: Manifestation of *bidromy*

D.A. Sadovskií, B.I. Zhilinskií*

Université du Littoral, UMR 8101 du CNRS, 59140 Dunkerque, France

Received 30 May 2006; accepted 26 September 2006
Available online 13 November 2006

Abstract

We consider a generalization of the 1:1:2 resonant *swing–spring* [see H. Dullin, A. Giacobbe, R.H. Cushman, Physica D 190 (2004) 15] which is suggested both by the symmetries of this system and by its physical and in particular molecular realizations [see R.H. Cushman, H.R. Dullin, A. Giacobbe, D.D. Holm, M. Joyeux, P. Lynch, D.A. Sadovskií, B.I. Zhilinskií, Phys. Rev. Lett. 93 (2004) 024302-1–024302-4]. Our generic integrable system is *detuned* off the exact Fermi resonance 1:2. The three-dimensional (3D) image of its energy–momentum map $\mathcal{EM}$ consists either of two or three qualitatively different non-intersecting 3D regions: a regular region at low vibrational excitation, a region with monodromy similar to that studied for the exact resonance, and in some cases—an intermediate region in which the 3D set of regular values of $\mathcal{EM}$ is partially self-overlapping while remaining connected. In the presence of this latter region, the system has an interesting property which we called *bidromy*. We analyze monodromy and bidromy for a concrete integrable classical Hamiltonian system of three coupled oscillators and for its quantum analog. We also show that the bifurcation involved in the transition from the regular region to the region with monodromy can be regarded as a special resonant equivariant analog of the Hamiltonian Hopf bifurcation.
© 2006 Elsevier Inc. All rights reserved.

Pacs: 33.20−t; 45.20−d; 05.45a

Keywords: Molecular vibrations; Integrable model; Nonlinear resonance; Quantum monodromy; Bidromy

Author's personal copy

* Corresponding author. Fax: +33328658244.
E-mail address: zhilin@univ-littoral.fr (B.I. Zhilinskií).

0003-4916/$ - see front matter © 2006 Elsevier Inc. All rights reserved.
doi:10.1016/j.aop.2006.09.011

1. Introduction

Hamiltonian systems with 1:1:2 resonance became recently of renewed acute interest after it was pointed out in [1] that they exhibited an interesting "plane switching" phenomenon, called so after the behavior which can be observed in the classical 1:1:2 resonant *swing–spring* or elastic pendulum with axial symmetry O(2) [2,3] (see Fig. 1, left). It was also shown in [3] that this behavior was intrinsically related to the *monodromy* [5,6] of integrable approximations to these systems. Furthermore, a quantum analog of the 1:1:2 resonant swing–spring was studied in [4], where its quantum monodromy [8,7] was interpreted as a particular one-dimensional defect of the three-dimensional (3D) lattice [9] whose nodes represented quantum eigenstates within the 3D image of the energy–momentum map $\mathcal{EM}$ of the corresponding classical system. The evidence that the CO_2 molecule (see Fig. 1) constitutes an almost perfect quantum 1:1:2 resonant swing–spring [10] opened perspectives of experimental manifestations of monodromy in molecules. In particular, the quantum plane switching phenomenon was demonstrated for CO_2 molecule [11].

1.1. Motivation for studying systems with detuned Fermi resonance

The Lie symmetry group G of the integrable approximation to the 1:1:2 resonant swing–spring system is a 2-torus group which includes the axial $\mathbb{S}^1$ symmetry (rotation about the vertical axis in Fig. 1) and the $\mathbb{S}^1$ symmetry defined by the flow of the 1:1:2 harmonic oscillator Hamiltonian. It can be easily shown (see Section 2) that any exactly 1:1:2 resonant system is exceptional within the class of G-invariant systems. Furthermore, while the frequencies of the 1:1 subsystem are exactly degenerate due to the axial symmetry, the 1:2 ratio between these frequencies and the frequency of the third oscillator, known as

personal copy

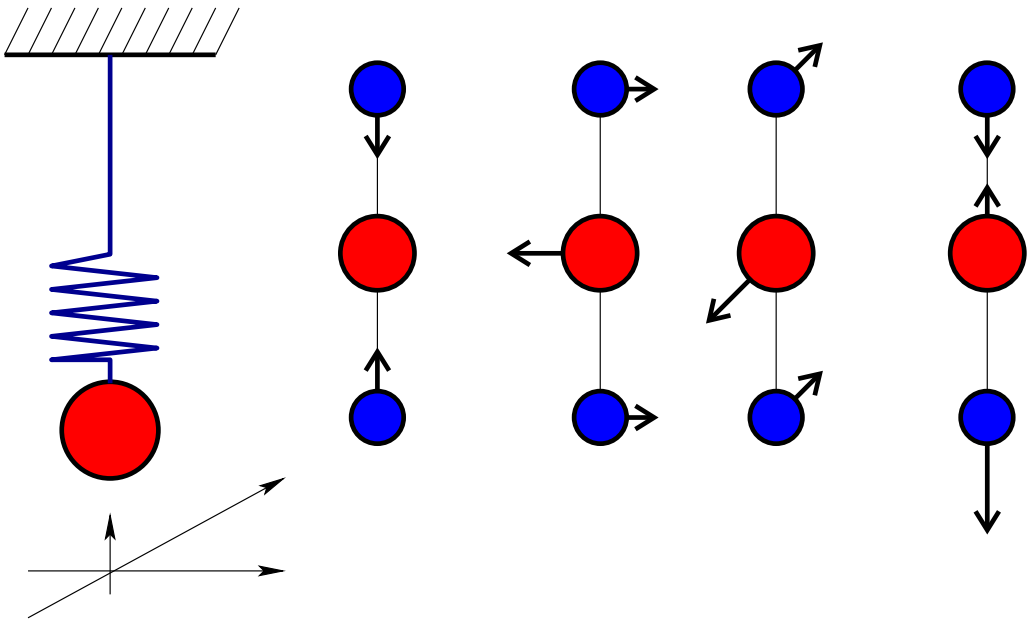

Fig. 1. Elastic pendulum and normal mode vibrations of the CO_2 molecule. Note that the first three modes, symmetric stretching v_1 and the two components of bending v_2 constitute the Fermi resonant oscillator system while the asymmetric stretch vibration v_3 is not in resonance and can be averaged out, see more in [10,4].

Fermi resonance, is not exact in real systems. So both symmetry arguments and physical realizations suggest studying a system with *detuned* Fermi resonance [12,13]. In this work we use the example of an integrable approximation to a classical system of three coupled nonlinear oscillators whose Hamiltonian may be regarded as an effective vibrational Hamiltonian of a linear triatomic molecule, such as CO_2 in Fig. 1.

1.2. Dynamical regimes of systems with detuned Fermi resonance

Our system has three first integrals, the integral N of the 1:1:2 resonant harmonic oscillator with value n, which we call *polyad integral*, the angular momentum L with value ℓ, and Hamiltonian H whose value, energy, we will denote by E; the image of the energy–momentum map $\mathcal{EM}$ of our system is a 3D region in the space $\mathbb{R}^3$ with coordinates (ℓ, E, n). The detuning term is part of the linearized Hamiltonian, i.e., this term is quadratic in (q,p). Since the main Fermi resonance term is of degree 3, it is clear that at very small n when our oscillator system is near its equilibrium $q = p = 0$, detuning is more important than the resonance interaction. In this region, which we call *regular*, the system can be globally described using three pairs of action-angle variables associated with its three normal oscillator modes. At the same time, detuning can be neglected at sufficiently high n. Dynamics in this high n region is qualitatively the same as that in the case of the exact resonance 1:1:2 studied in [3] and the joint eigenvalue spectrum lattice of the corresponding quantum system should be equivalent to that described in [4]. In particular, our system should have monodromy and consequently, it cannot be described using global action-angle variables.

1.3. Transition between different dynamical regimes

It is commonly known that in a parametric family of systems with two degrees of freedom, transition from a regular system to a system with monodromy is often associated with *Hamiltonian Hopf bifurcation* [14]. In our situation, the most directly relevant generalization of this bifurcation to three degrees of freedom is that of a bifurcation of a relative equilibrium (RE) which is an orbit of an $\mathbb{S}^1$ action. However, in all cases studied up to now [15–20] the bifurcating orbit was a regular orbit of a locally free $\mathbb{S}^1$ action and after the $\mathbb{S}^1$ symmetry was reduced the RE became an equilibrium undergoing a standard Hamiltonian Hopf bifurcation. So, though clearly important for many applications, such generalization is somewhat trivial. The major difference of our situation is that the bifurcating orbit is an isolated critical orbit of the particular $\mathbb{S}^1$ action of the 1:1:2 resonant harmonic oscillator system. This orbit corresponds to the pure "spring" motion described by the oscillator with frequency 2. (Note that in the CO_2 molecule it corresponds to the symmetric stretch vibration v_1.) All other orbits are generic and are two times longer. The short orbit is stable in the regular region (at low n); it turns unstable as n increases past n_{crit}. We show that this bifurcation is in many ways reminiscent of the trivial generalization of the Hamiltonian Hopf bifurcation to RE. However, it cannot be reduced to the standard case because, obviously, the bifurcating RE becomes a singular point after our $\mathbb{S}^1$ action gets reduced. In order to underline the nontrivial way in which the $\mathbb{S}^1$ symmetry becomes involved, we speak of resonant equivariant generalization of the Hamiltonian Hopf bifurcation to RE.

In what follows we consider the 3D-image of the $\mathcal{EM}$ map as a one-parameter family of 2D-images parameterized by the value n of the polyad integral. To understand the global picture we split the whole range of $n > 0$ into regions where the $\mathcal{EM}$ images (for fixed n) do

Author's personal copy

not vary qualitatively. We are not interested in the trivial exceptional value $n = 0$. We are interested only in modifications of the $\mathcal{EM}$ image closely related to the bifurcation of the "spring" RE. We do not take into account possible saddle-node bifurcations [27–29] which can lead to the appearance of new RE and to more complex intra-polyad dynamics but do not involve the local neighborhood of the "spring" RE.

1.4. Supercritical transition

We aim at describing the whole of the image and fibers of the $\mathcal{EM}$ map of our system, and therefore we should go beyond studying the resonant bifurcation of the "spring" RE as a purely local individual phenomenon. Much like the standard Hamiltonian Hopf bifurcation [14], this bifurcation can be of two types depending on the parameters of the high order terms in the Hamiltonian. Keeping the terminology, we call them *supercritical* and *subcritical*.

The global context of the supercritical bifurcation is quite simple. There is no other related phenomena and the 3D-image of the $\mathcal{EM}$ map can be split (depending on n value) into two non-intersecting 3D-domains and one exceptional 2D-section. One of these 3D-domains belongs to the region $0 < n < n_{\text{crit}}$, the other domain lies in the region $n > n_{\text{crit}}$. The exceptional section of the $\mathcal{EM}$ map for $n = n_{\text{crit}}$ includes the image of the fiber corresponding to the short "spring" RE at the moment of bifurcation. Note that because of somewhat less stringent conditions on the Hamiltonian parameters, this kind of global structure of the $\mathcal{EM}$ image seems to be prevailing in real molecular systems. CO_2 is certainly of this kind. However the bifurcation happens there at very low value of n which is far below $n = \frac{3}{2}$ of the ground state of the quantum analog and hence is unobservable. On the other hand, the CS_2 molecule with much larger detuning provides a good example.

1.5. Subcritical transition and bidromy

The subcritical scenario of the transition from the regular normal mode region to the monodromy region is more complicated. In this case, the resonant Hopf-like bifurcation of the short "central" or "spring" RE at $n = n_{\text{crit}}$ is preceded by two equivalent-by-symmetry cusp bifurcations at $n = n' < n_{\text{crit}}$ which give rise to new RE. In the small region with $n' < n < n_{\text{crit}}$, the 3D set $\mathsf{R}_{\mathcal{EM}}$ of regular $\mathcal{EM}$ values *folds over itself while remaining connected* thus forming a third *transitional region*. All this happens "semi-globally" in the small immediate vicinity of the spring RE and the whole sequence of bifurcations is predefined or "organized" by the form of the Hamiltonian. Most importantly, this sequence of bifurcations and the geometry of the image and fibers of the $\mathcal{EM}$ map in the transitional region are *structurally stable* with regard to any sufficiently small equivariant variations of the Hamiltonian.

The fact that the inverse map $\mathcal{EM}^{-1}$ becomes multi-component shortly before or after a subcritical bifurcation occurs has been observed in a number of different systems [16,17,20,23] and seems to be a common feature. In all these cases the set $\mathsf{R}_{\mathcal{EM}}$ of regular values in the image of the $\mathcal{EM}$ map can be represented using a *cell unfolding surface* $\mathsf{S}_{\mathcal{EM}}$. Different points of this surface which have the same energy E and momenta $(n, \ell, \ldots)$ represent different regular connected components (normally tori) of the fiber $\mathcal{EM}^{-1}(E, n, \ell, \ldots)$. Such representation is especially simple in the two-dimensional case.

Author's personal copy

Note that the closure $\bar{\mathsf{S}}_{\mathcal{EM}}$ represents all (i.e., both regular and critical) $\mathcal{EM}$ values and that such construction is similar to that of Riemann surfaces and branch coverings.

1.5.1. Overlapping lower cells

In all cases we have so far encountered in the literature [20–23,25,26], the two-dimensional surface $\bar{\mathsf{S}}_{\mathcal{EM}}$ consists of several disconnected sheets glued together along a set of critical $\mathcal{EM}$ values. We will name these sheets *lower cells* (for a general discussion of lower cells see Section 2 of [24]). Thus consider a simple example of three lower cells in the image of the $\mathcal{EM}$ map of which two cells overlap (partially) as shown in Fig 2. The cells are glued together along the line of critical values c, which either ends at the boundary of the $\mathcal{EM}$ image or goes to infinity (cf.[26]). The singular fiber $\mathcal{EM}^{-1}(c)$ is a "bi-torus" which can be modeled in three dimensions as two tori glued together along one of their principle circles. In Fig. 2 we also show two regular $\mathcal{EM}$ values a and b. The former lifts to one regular torus $\mathcal{EM}^{-1}(a)$, while the latter is in the overlap area of two lower cells and the fiber $\mathcal{EM}^{-1}(b)$ consists of *two* tori. On the unfolding surface, b corresponds to b' and b''. A somewhat different situation occurs if one of the ends of the singular line is not connected to any boundary (see Fig. 3, left). In this case we have two lower cells, the values a and b' lie on the same sheet of $\mathsf{S}_{\mathcal{EM}}$ and can be connected by a continuous path in the set of regular $\mathcal{EM}$ values. Furthermore, if *both* ends of the gluing segment of singular $\mathcal{EM}$ values c do not connect to any boundary (see Fig. 3, right), then the sheet containing a and b' is not simply connected. In this case the system may have nonlocal monodromy computed along a noncontractible path around the singular segment. This situation was discussed in relation to a quadratic deformation of the spherical pendulum [23] and its particular molecular realization [25], as well as in the two-center system [21,22]. Due to extra discrete symmetries, there are two "small" sheets glued to the critical segment in the case of the subcritical Hopf bifurcation of the hydrogen atom in crossed electric and magnetic fields [20]. Note that systems studied in [21,22,20] have an extra degree of freedom and that their lower cells are three-dimensional and that the path $a{-}(b'){-}a$ remains noncontractible in the full 3D image of their $\mathcal{EM}$ map.

1.5.2. Self-overlapping lower cell

Our present case is also three-dimensional. When the bifurcation of the spring RE is subcritical it has many similarities with [21,22] albeit *one important difference*: while

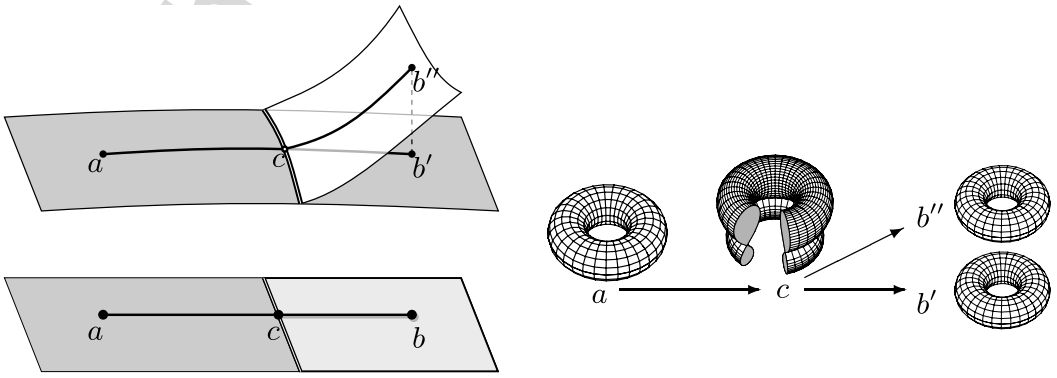

Fig. 2. Example of overlapping lower cells in the 2D-image of the energy–momentum map $\mathcal{EM}$: a multi-sheet cell unfolding surface (top left) and the corresponding $\mathcal{EM}$ image (bottom). Points a, b', b'', and c lift each to one connected component of the integrable fibration shown right; b' and b'' correspond to the same $\mathcal{EM}$ value b.

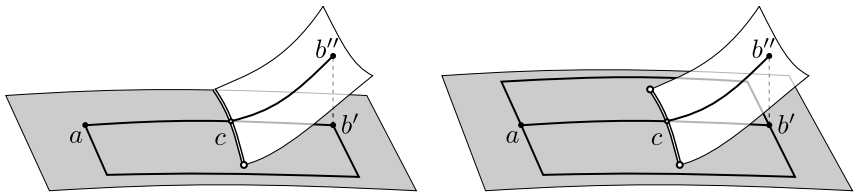

Fig. 3. Possible two-sheet cell unfolding surfaces for the image of an $\mathcal{EM}$ map with two overlapping lower cells, cf. Fig. 2. Fibers in the image of $\mathcal{EM}^{-1}$ can have either one (a) or two (b' and b'') connected components; a and b' can be related by a continuous path which lies in the set of regular $\mathcal{EM}$ values of the "lower" (grey) sheet. In the case of the right surface, this sheet is not simply connected and the system has monodromy.

$\mathcal{EM}^{-1}$ becomes two-valued in the part of the transitional region, the set of regular values of the surface $\mathsf{S}_{\mathcal{EM}}$ *remains connected*. In other words, we deal with one single self-overlapping lower cell and $\mathsf{S}_{\mathcal{EM}}$ consists of one sheet as illustrated in Fig. 4 in the two-dimensional case. It can be seen that now *both* points b' and b'' can be connected by a path going through the set of regular $\mathcal{EM}$ values. Since b' and b'' represent one value, this path is closed in the image of the $\mathcal{EM}$ map, but it is not closed on $\mathsf{S}_{\mathcal{EM}}$.

This specific feature of the image of the $\mathcal{EM}$ map, namely the existence of the region of values whose preimage consists of two disconnected components (tori) which can be connected by a smooth path going only through regular tori allows us to introduce the new concept of *bidromy*. Standard integral Hamiltonian monodromy characterizes the evolution of the first homology group of the regular fiber along a closed (non-contractible) path going only through regular tori. "Fractional monodromy" which was introduced recently [30,24] is a generalization which allows for closed paths to cross certain singular tori (the so called curled tori). With the concept of bidromy announced recently in [31] we attempt further generalization. Namely, we study paths which start at point a (see Fig. 4), then approach the line of critical values and bifurcate in point c of this line (recall that c represents a bitorus) into two paths which fuse together after going in two different ways and join the initial point a, thus forming the closed "bipath". The bidromy is the tentative generalization of monodromy to a special class of "bipaths". In order to realize such a generalization we need to define a suitable class of homotopically equivalent closed "bipaths", which allow the transportation of the basis cycles of some subgroup of the first homology group of a regular fiber along such closed "bipaths" and to show that the transformation between initial and final system of cycles does not depend on the concrete choice of "bipaths" within the chosen class of homotopically equivalent "bipaths". Naturally, the manifestation of classical "bidromy" in corresponding quantum problems should be studied in parallel because, as it was mentioned earlier on several occasions [4,16,30,24,31], the complementarity of classical and quantum points of view allows better understanding of both phenomena.

Author's personal copy

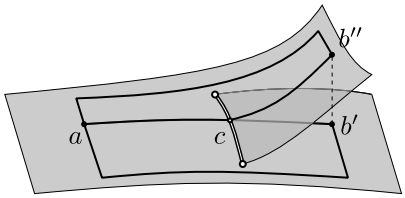

Fig. 4. A single-sheet cell unfolding surface for the image of an $\mathcal{EM}$ map with one self-overlapping lower cell: the inverse map $\mathcal{EM}^{-1}$ can have one (point a) or two (points b' and b'') connected components, cf. Fig. 2.

Our main result in this paper is the construction of a relatively simple model exhibiting this new phenomenon. Our model describes the internal polyad structure of vibrational polyads formed by three nonlinear vibrational modes in 1:1:2 resonance in the presence of axial symmetry with small detuning between doubly degenerate mode and nondegenerate mode with double frequency. We give detailed analytical description of the corresponding classical problem, pay special attention to the stratification of the image of the $\mathcal{EM}$ map, and demonstrate characteristic features of the joint energy–momentum spectrum for the corresponding quantum problem.

The organization of the paper is as follows. We remind in Section 2 using a concrete example of three-dimensional system of nonlinear 1:1:2 resonant oscillators the general scheme of the qualitative analysis of classical dynamical systems based on construction of integrable models, their reduction, and geometrical representation. Section 3 describes the construction via appropriate scaling transformation of the simplified universal model valid in the narrow region where the qualitative modifications of the image of the $\mathcal{EM}$ map take place. The results of the analysis of the 3D-image of the corresponding $\mathcal{EM}$ map are given in Section 4 through geometrical representation of different 2D-sections in order to visualize better the 3D-region responsible for the presence of monodromy and bidromy for this problem. Complete analytical solution for all strata on the 3D-image of the $\mathcal{EM}$ map is given in the Appendix A. Section 5 introduces the system of closed paths and ''bipaths'' associated with monodromy and ''bidromy'' of the classical model system. Corresponding quantum problem and the manifestation of classical ''bidromy'' in quantum system is discussed in Section 6. Section 7 briefly discusses possible physical systems which seem to be the most realistic candidates to observe the manifestation of quantum bidromy and possible ways of further mathematical clarification and simplification of bidromy transformations.

2. Generic axially symmetric integrable Fermi resonant system

The logic behind defining our generic 1:1:2 system and constructing its integrable model is as follows:

(i) state all symmetries, geometric (exact) and dynamical (possibly approximate), which constitute the total two-parameter Lie symmetry group G of the system with two integrals (N, L);
(ii) consider sections $\mathcal{O}_{n,\ell}$ of the orbit space $\mathcal{O}$ of the action of G on the original phase space $\mathbb{R}^6$ with coordinates (q,p) for given fixed values (n,ℓ) of first integrals (N,L);
(iii) define the ring $\mathcal{R}$ of all polynomials in dynamical variables (q,p) which are G-invariant; use these polynomials to represent $\mathcal{O}_{n,\ell}$ which are called reduced phase spaces $P_{n\ell}$;
(iv) assume that the Hamiltonian H of the system is a power series in (q,p) where the coefficients in front of the terms of total degree k in (q,p) can be scaled using a universal smallness parameter $\epsilon < 1$ as ϵ^{k-2};
(v) assume that H is G-invariant (or can be made such by normalization) and therefore H (or its normal form $\mathcal{H}$) belongs to $\mathcal{R}$ and that for any given k it can include all possible polynomials of degree k from $\mathcal{R}$;
(vi) verify that the family of constant energy-level sets of H on $P_{n,\ell}$ is *structurally stable* with respect to any sufficiently small G-equivariant change of H.

Author's personal copy

Below we follow this outline. Instead of (q,p) we will use the usual complex Hamiltonian coordinates

$$z = q - \mathrm{i}p, \quad \bar{z} = q + \mathrm{i}p, \quad \{z, \bar{z}\} = 2\mathrm{i},$$

which are more convenient to study the action of G.

2.1. Exact symmetries

The geometric axial symmetry C_∞ of the system results in the exact first integral, the angular momentum

$$L = \tfrac{1}{2}(z_2\bar{z}_3 - \bar{z}_2 z_3)\mathrm{i}, \tag{1}$$

whose value will be denoted by ℓ. We assume also additional discrete time reversal symmetry which acts on z variables like involution $z \to \bar{z}$. Under this operation L transforms as $L \to -L$.

2.2. Approximate dynamical symmetry

To account for the dynamical $\mathbb{S}^1$ symmetry of the Fermi system, we introduce the approximate first integral N

$$N = \bar{z}_1 z_1 + \tfrac{1}{2}\bar{z}_2 z_2 + \tfrac{1}{2}\bar{z}_3 z_3 = 2n_1 + (n_2 + n_3), \tag{2}$$

which is the harmonic oscillator Hamiltonian, whose flow generates the $\mathbb{S}^1$ symmetry of the 1:1:2 resonance; we call *N polyad integral* (a terminology inherited from quantum analogs of these systems) and we denote its value by n.

2.3. Hamiltonian in terms of invariant polynomials

The reduced system can be described fully using three dynamical variables [4]

$$R = \tfrac{1}{2}\bar{z}_2 z_2 + \tfrac{1}{2}\bar{z}_3 z_3 = (n_2 + n_3), \tag{3a}$$

$$S = \tfrac{1}{4}(\bar{z}_1 z_3^2 + z_1\bar{z}_3^2 + z_1\bar{z}_2^2 + \bar{z}_1 z_2^2), \tag{3b}$$

$$T = \tfrac{1}{4}(\bar{z}_1 z_3^2 - z_1\bar{z}_3^2 - z_1\bar{z}_2^2 + \bar{z}_1 z_2^2)\mathrm{i}, \tag{3c}$$

which are all invariants of the 1:1:2 oscillator action and are submitted to relation

$$2\Phi_{n,\ell} = T^2 + S^2 - [R^2 - \ell^2](n - R) = 0, \tag{4a}$$

and inequalities

$$n \geqslant R \geqslant |\ell| \geqslant 0. \tag{4b}$$

It should be also noticed that the reduced system inherits additional finite symmetry properties from the original system, notably the invariance with respect to $\ell \to -\ell$ and $T \to -T$. Taking these further symmetries and Eq. (4a) into account, we can show that $\mathcal{H}_{n,\ell}$ is an arbitrary polynomial in just *two* invariants R and S and that it includes only even degrees in ℓ.

Author's personal copy

2.4. Reduced phase space

The phase space $P_{n,\ell}$ of the reduced system is compact. Specifically, it is just a point when either $n=0$ or $|\ell|=n=\ell_{\max}$, it is diffeomorphic to a smooth sphere $\mathbb{S}^2$ for $0<|\ell|<n$, while for $\ell=0$ (and $n>0$) this space is a sphere with one conical singular point (a "turnips"). We represent $P_{n,\ell}$ in the ambient space $\mathbb{R}^3$ with coordinates (S,T,R) using Eq. (4). We can easily see that $P_{n,\ell}$ is a surface of revolution about axis R and that it suffices to consider a projection of $P_{n,\ell}$ on a plane which contains this axis. The plane $\{T=0\}$ chosen in Fig. 5 is particularly convenient in view of the discrete symmetry $T\to -T$ of the reduced Hamiltonian $\mathcal{H}_{n,\ell}$.

To characterize the singularity of P_{n0} at $R=S=T=0$, notice that near this point

$$T^2+S^2\approx nR^2,$$

and therefore P_{n0} is tangent to a cone with angle $2\tan^{-1}2\sqrt{n}$ which intersects $\{T=0\}$ in two rays $S=\pm\sqrt{n}R,\quad R\geqslant 0$.

2.5. Model Hamiltonian

In order to construct now the integrable Hamiltonian which preserves exact geometrical symmetry and approximate dynamic symmetry we can use the polynomial expansion of the Hamiltonian in terms of dynamical variables R, S introduced in previous section and in terms of integrals of motion N, L. Moreover, replacing initial six-dimensional phase space by two-dimensional family of reduced phase spaces parameterized by two values (n,ℓ) of integrals N, L, we can rewrite Hamiltonian in terms of a power series in R, S with coefficients depending on values (n,ℓ) of two integrals of motion.

$$H=E_0(n,\ell)+a(n,\ell)S-b(n,\ell)R+c(n,\ell)R^2+\cdots \tag{5}$$

Each doubly reduced Hamiltonian for fixed (n,ℓ) values is given on the corresponding two-dimensional reduced phase space which is defined in the three-dimensional space of invariant polynomials R, S, T by syzygy (4a) depending on n and ℓ values. In order to describe the qualitative features of the system we need to analyze the intersection of the reduced phase space by the constant levels of the Hamiltonian. As soon as Hamiltonian does not depend on T it is sufficient to study only the intersection of the constant energy level of the Hamiltonian $H=\text{const}$ with the boundary of the $T=0$ section of the doubly reduced phase space which is given by equation

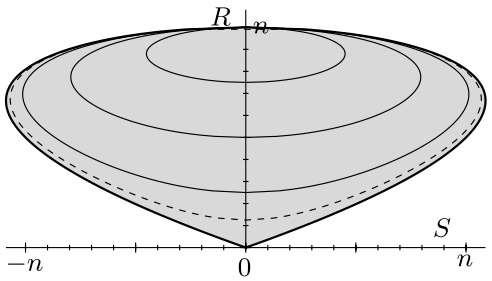

Fig. 5. Reduced phase spaces $P_{n\ell}$ of the 1:1:2 resonant systems with axial symmetry shown as projections $V_{n\ell}$ on the $\{T=0\}$ plane. Shaded area represents the singular space with $\ell=0$; other contours show boundaries of $V_{n\ell}$ with $\ell/\ell_{\max}=\frac{1}{8}$ (dashed line), $\frac{1}{4}$, $\frac{1}{2}$, and $\frac{3}{4}$.

Author's personal copy

$$S^2 = (R^2 - \ell^2)(n - R). \tag{6}$$

Thus, the mathematical problem of characterizing qualitative modification of the constant energy levels under variation of E, ℓ, n consists in the study of solutions of two polynomial equations (5) and (6).

2.6. Critical behavior and structural stability

Both, the reduced phase space and the constant energy level set are two-dimensional surfaces in the 3D space of invariant polynomials (R, S, T). Thus generically, an intersection of reduced phase space and the constant energy level consists of one or of several closed curves. But due to the fact that the constant energy level is independent on T and the reduced phase space in R, S, T variables has very simple axially symmetric geometrical form it is sufficient to study the intersection of the projection of $P_{n\ell}$ on $T = 0$ plane with $E_{n,\ell}(R, S) = \text{const}$ level. This intersection can become exceptional due to two different reasons:

(i) the intersection includes the singular point $R = 0$, $S = 0$ of the reduced phase space $P_{n\ \ell=0}$, which is possible only for $\ell = 0$ case;
(ii) level set $E_{n,\ell}(R, S) = \text{const}$ is tangent to the boundary of the reduced phase space.

Nevertheless, as soon as both, constant energy level set and reduced phase space, are n dependent, it is possible that within the n-dependent family there exists some special "critical" value of $n = n_{\text{crit}}$ for which the two abovementioned reasons are simultaneously satisfied. Namely, for $n = n_{\text{crit}}$ the intersection includes the singular point $R = 0$, $S = 0$ and at that point the constant energy level set $E_{n,\ell=0}(R, S) = \text{const}$ is tangent to the boundary of the projection of the phase space on the $T = 0$ plane. The so obtained $n = n_{\text{crit}}$ value corresponds to the bifurcation of the energy–momentum map because if for $n \leqslant n_{\text{crit}}$ the exceptional intersection, which includes the singular $R = 0$, $S = 0$ point, belongs to the boundary of the $\mathcal{EM}$ map, then for $n > n_{\text{crit}}$ the value of the $\mathcal{EM}$ map corresponding to exceptional intersection lies inside the $\mathcal{EM}$ map. Fig. 6 shows three different situations which can occur when the family of constant energy levels intersect the boundary of the projection of the reduced phase space on the $T = 0$ plane. This figure oversimplifies the real situation because the constant energy levels and the boundary are represented in the linearized form. Fig. 6(b) shows clearly that in the linear approximation the intersection of the constant energy level with phase space boundary at $n = n_{\text{crit}}$ is not generic. One needs to take into account second order terms to make the situation structurally stable.

We are primarily interested in the qualitative modification which takes place at the critical point $n = n_{\text{crit}}$ and in any other related qualitative modifications which can appear in the neighborhood of $n = n_{\text{crit}}$.

In order to construct the mathematical model which keeps all important terms needed to describe the generic behavior around the critical point, we can neglect all dependence of the terms of Hamiltonian on n, ℓ and restrict ourselves with the following system:

$$H = aS - bR + cR^2; \qquad a > 0, \quad b > 0, \tag{7a}$$

$$S^2 = (R^2 - \ell^2)(n - R). \tag{7b}$$

Authors Personal Copy

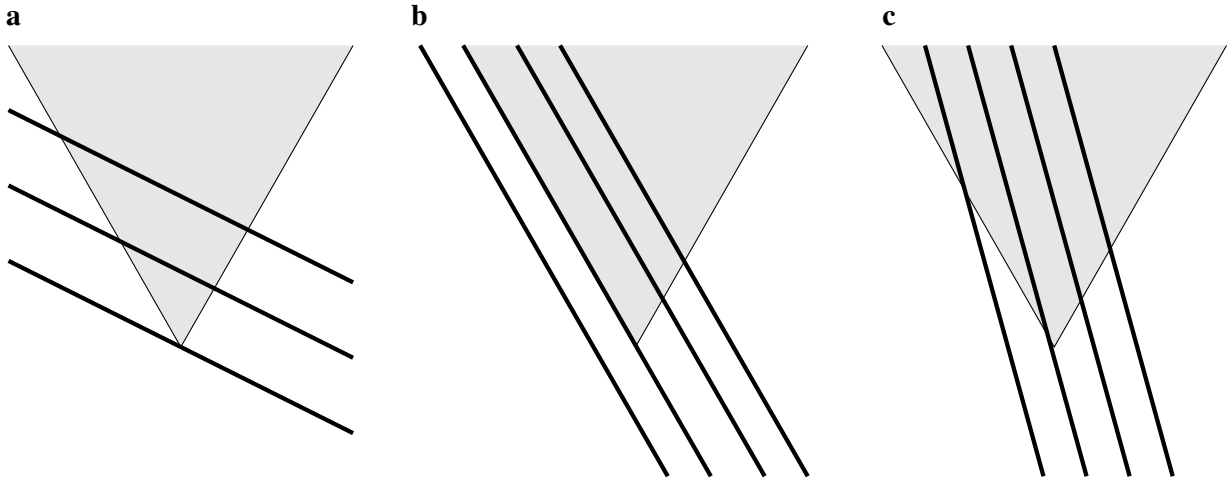

Fig. 6. Schematic view (linear approximation for reduced phase space boundary and for energy level) of a family of constant energy levels which crosses reduced phase space. Three different cases are plotted: (a) Critical value of the $\mathcal{EM}$ map associated with singular point of the reduced phase space lies on the boundary of the image of $\mathcal{EM}$ map; (b) Exceptional intersection is tangent to the boundary at singular point; (c) Critical value of the $\mathcal{EM}$ map associated with singular point of the reduced phase space lies inside the image of $\mathcal{EM}$ map.

Here, we assume that the constant energy level does not depend explicitly on n and ℓ. At the same time the boundary of the reduced phase space in R, S variables depends on both n and ℓ. Restriction of the Hamiltonian expansion (7a) up to quadratic in R terms (quartic terms in initial p, q variables) is sufficient to ensure its structural stability under small deformation. The resonance model without detuning follows from Eqs. (7a) and (7b) by putting $b = c = 0$.

3. Scaling transformation near critical point

To see the qualitative structure of the image of the $\mathcal{EM}$ map we need to analyze the common level sets of H and of two integrals of motions, N and L. The point $R = 0$, $S = 0$ is the special singular point of the $\ell = 0$ reduced phase space for any n. Its stabilizer has additional finite Z_2 symmetry. If the $H = E$ constant energy-level set includes this point, the corresponding value $(E, n, \ell = 0)$ is a critical value of $\mathcal{EM}$. Depending on the coefficients in (7a) the constant energy level which passes through the $R = S = 0$ point can consist of this point only or can consist of a whole family of points of the reduced phase space. In order to distinguish between these two important cases we need to compare the slope of the energy level with the slope of the boundary of the phase space at the same point $R = S = 0$ and to be more precise to compare as well the second derivatives at the same point.

For the first derivatives we have:

$$\left.\frac{\mathrm{d}S^{\mathrm{En.L}}}{\mathrm{d}R}\right|_{R=0,\ell=0} = \frac{b}{a}, \tag{8a}$$

$$\left.\frac{\mathrm{d}S^{\mathrm{b}}}{\mathrm{d}R}\right|_{R=0,\ell=0} = \sqrt{n}. \tag{8b}$$

where $S^{\mathrm{En.L}}$ and S^{b} are, respectively, expressions for S found from energy level (7a) and from reduced space boundary (7b). We suppose below that coefficients a, b in (7a) are positive.

Authors personal

In a similar way for the second derivatives we have:

$$\left.\frac{\mathrm{d}^2 S^{\mathrm{En.L}}}{\mathrm{d}R^2}\right|_{R=0,\ell=0} = -\frac{2c}{a}, \tag{9a}$$

$$\left.\frac{\mathrm{d}^2 S^{\mathrm{b}}}{\mathrm{d}R^2}\right|_{R=0,\ell=0} = -\frac{1}{\sqrt{n}}. \tag{9b}$$

When n increases (n is positive by physical reasons) the slope of the boundary increases and at certain $n = n_{\mathrm{crit}}$ it becomes equal the slope of the energy level. This means that for $n < n_{\mathrm{crit}}$ the critical value belongs to the boundary of the energy–momentum map, whereas for $n > n_{\mathrm{crit}}$ the critical value lies inside the energy–momentum map. The corresponding fibers are also naturally qualitatively different. To precise the structure of corresponding fibers we need to look for the value of second derivatives.

Depending on the relative values of second derivatives two different scenarios occur in the neighborhood of the $n = n_{\mathrm{crit}}$ value.

As soon as we want to analyze the qualitative modifications which occur when n changing around $n = n_{\mathrm{crit}}$ it is useful to introduce n_{crit} explicitly and consider small deviations from it $x = n - n_{\mathrm{crit}}$ in the model equations together with the critical value c_{crit} of the second derivatives and small relative deviations from it $c = c_{\mathrm{crit}}(1 + y)$, which we denote as y.

From (8a), (8b), (9a) and (9b) we find

$$n_{\mathrm{crit}} = \frac{b^2}{a^2}, \quad c_{\mathrm{crit}} = \frac{a^2}{2b}. \tag{10}$$

Now we replace in the model system (7a), (7b) n and c by n_{crit}, c_{crit}, and x and y characterizing small deviations from n_{crit} and c_{crit}.

$$H = aS - bR + \frac{a^2}{2b}(1 + y)R^2; \tag{11a}$$

$$S^2 = \left(R^2 - \ell^2\right)\left(\frac{b^2}{a^2}(1 + x) - R\right). \tag{11b}$$

We introduce now scaling transformation

$$R \to \frac{b^2}{a^2}R; \quad S \to \frac{b^3}{a^3}S; \quad H \to \frac{b^3}{a^2}H; \quad \ell \to \frac{b^2}{a^2}\ell, \tag{12}$$

which puts the model system (7a), (7b) into a simple form:

$$H = S - R + \frac{1 + y}{2}R^2; \tag{13a}$$

$$S^2 = (R^2 - \ell^2)(1 + x - R). \tag{13b}$$

From the point of view of further formal analysis of the model it turns out that it is suitable to change the parameterization and to introduce instead of y another parameter

$$u = (2y + 1)^{1/6}, \quad y = (u^6 - 1)/2. \tag{14}$$

Finally with new parameter u introduced, the system of equations defining the energy level and the boundary of the "reduced phase space" has the following form:

Author's personal copy

$$H = S - R + \frac{u^6 + 1}{4} R^2; \tag{15a}$$

$$S^2 = (R^2 - \ell^2)(1 + x - R). \tag{15b}$$

The rest of the paper is essentially the mathematical analysis of the model defined by Eqs. (13a) and (13b) or by Eqs. (15a) and (15b) in the u-parameterization and the interpretation of the results of this analysis from the point of view of qualitative features of corresponding classical dynamical system and its quantum analog.

4. Geometrical analysis of the energy–momentum map

By definition, the parameter value $x = 0$ corresponds to $n = n_{\text{crit}}$ and characterizes the bifurcation point. Near $x = 0$ the scenario of the bifurcation depends on the value of y or, equivalently, on u in the u-parameterization.

In the case of $y < 0$ (or $u < 1$) under variation of x near $x = 0$, the critical value which was on the boundary of the image of $\mathcal{EM}$ map for $x < 0$ becomes an internal point for $x > 0$. We name the corresponding bifurcation *supercritical*.

In the case of $y > 0$ (or $u > 1$) the scenario is more complicated. At $x < 0$ but sufficiently close to $x = 0$ the inverse image of the energy–momentum map corresponding to critical value consists of two disconnected components. This means that there are two disconnected fibers of the $\mathcal{EM}$. One of these two fibers contains critical point and the image of the $\mathcal{EM}$ map for this system of fibers has the critical value on the boundary of the image of $\mathcal{EM}$ map.

At $x = 0$ one of two components disappears and for $x > 0$ only one component is present in the inverse image of the $\mathcal{EM}$ map. For $x > 0$ the critical value is inside the image of the $\mathcal{EM}$ map. We name such bifurcation *subcritical*.

In the case of small positive values of y (u is slightly greater than 1) the second component in the inverse image of the $\mathcal{EM}$ map appears only for negative x close to zero.

In order to characterize now the critical values of the $\mathcal{EM}$ map we need to find points at which constant energy level given by (15a) touches the boundary of the phase space given by (15b). We need also to distinguish between touching points of first, second and third order. For the three dimensional image of $\mathcal{EM}$ the touching points of third order correspond to exceptional (zero-dimensional) critical values. Touching points of second order correspond to critical values forming one-dimensional lines. At last, first order touching points correspond on the 3D-image of $\mathcal{EM}$ to 2D-boundary regions of critical values.

In order to understand better the 3D-structure of the image of the $\mathcal{EM}$ map we start with its geometrical representation for some typical value of parameter y or u. Detailed analytical expressions for different strata on the image of $\mathcal{EM}$ are given in Appendix A.

4.1. $\ell = 0$ section of the image of $\mathcal{EM}$

Let us begin by plotting several 2D-sections of the image of $\mathcal{EM}$ map. The global view of the $\ell = 0$ section is shown in Fig. 7.

To see the behavior of the line of singular values near the $E = 0$, $x = 0$ point in more detail we change the scale and represent only critical values corresponding to critical points due to first-order-touching between energy level and the boundary of the reduced

Author's personal copy

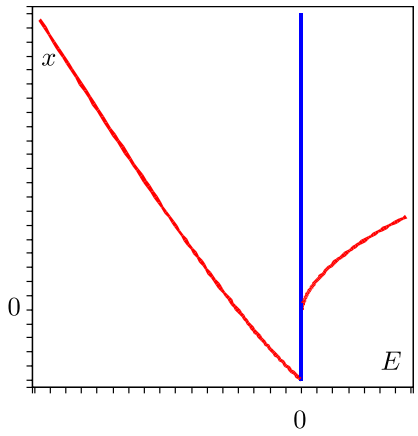

Fig. 7. Global view of the image of energy-momentum map for $\ell^2 = 0$ calculated for $y = 1/10$ or $u = (1 + 2/10)^{1/6}$. The $E = 0$ line corresponds to the critical values associated with the singular point $S = R = 0$ of the reduced phase space.

space. Depending on the sign of y or on the sign of $u - 1$ in the u-parameterization scheme (15), the image of the energy–momentum map has qualitatively different form.

In the case of positive y (or equivalently $u > 1$) there are two bifurcation points (points B and O in Fig. 8) on the image of the $\mathcal{EM}$ map. First bifurcation (point B) occurs at small non-zero negative values of $E = E_B$ and $x = X_B$, corresponding to $R = R_B$. At this point the degenerate touching point between the energy level and the boundary of the reduced space is formed and two families of ordinary touching points bifurcate as x increases. In the total space this corresponds to appearance of the second disconnected component of the $\mathcal{EM}$ map which we will name the "second fiber". One of these new families of relative equilibria approaches the singular value $E = x = 0$ and disappears at point O after colliding with symmetry imposed critical value. All that can be seen in Fig. 8.

In the case of non-positive y (or equivalently $u \leqslant 1$) there is only one bifurcation point O at $E = x = 0$. At this point new family of relative equilibria bifurcates from the singular critical value of the image of $\mathcal{EM}$ map. This situation is shown in Fig. 9.

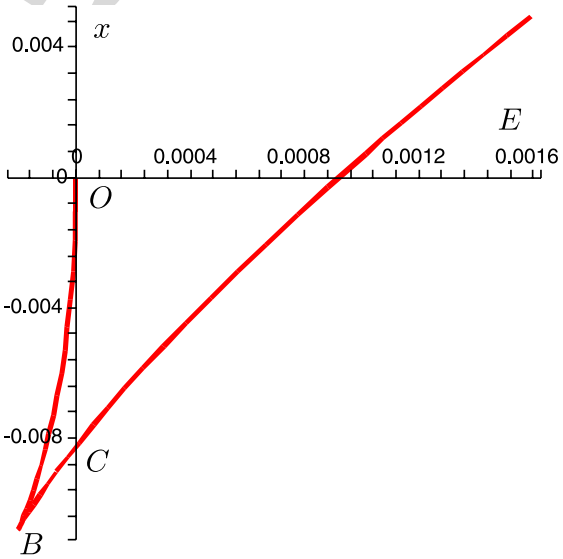

Fig. 8. Blowup of Fig. 7. Singular values of the energy–momentum map for $\ell^2 = 0$. Model calculation with $y = 1/10$ or $u = (1 + 2/10)^{1/6}$.

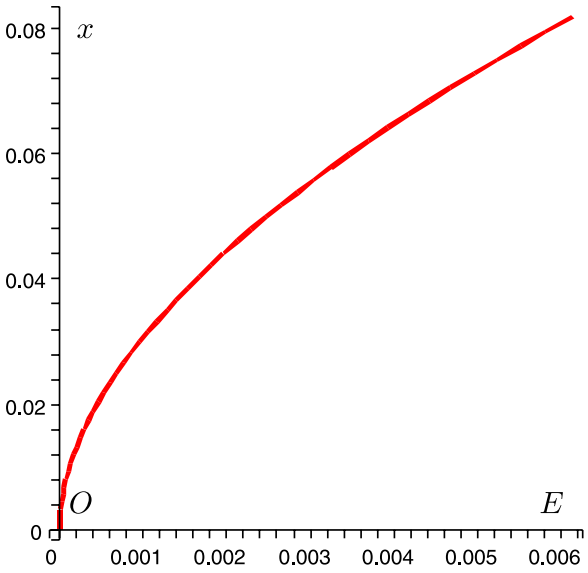

Fig. 9. Singular values of the energy–momentum map for $\ell^2 = 0$. Model calculation with $y = -1/10$ or $u = (1 - 2/10)^{1/6}$.

4.2. Arbitrary ℓ = const and x = const sections of $\mathcal{EM}$

The graphical representation of critical lines on the image of $\mathcal{EM}$ map for different $\ell^2 = \text{const}$ sections of the 3D-image is shown in Fig. 10. Every regular point on this line of critical values corresponds to simple touching between energy level and boundary of the reduced space for corresponding ℓ^2 value. Two singular cusp points for each $\ell^2 = \text{const}$ section correspond to second order touching (both first and second derivatives coincide). If we further increase the ℓ^2 value, these two singular points become closer to each other and at some particular value of ℓ^2 they coincide (point A in Fig. 11). The corresponding ℓ^2 value specifies with the reduced space which allows the third order touching between energy

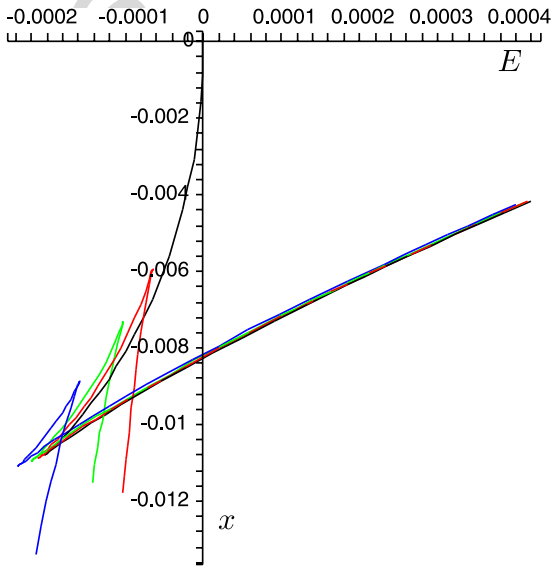

Fig. 10. Sections of energy–momentum space by $\ell^2 = 0$ (black), $\ell^2 = 10^{-6}$ (red), $\ell^2 = 2 \times 10^{-6}$ (green) and $\ell^2 = 4 \times 10^{-6}$. Model calculation with $y = 1/10$. (For interpretation of the references to color in this figure legend, the reader is referred to the web version of this paper.)

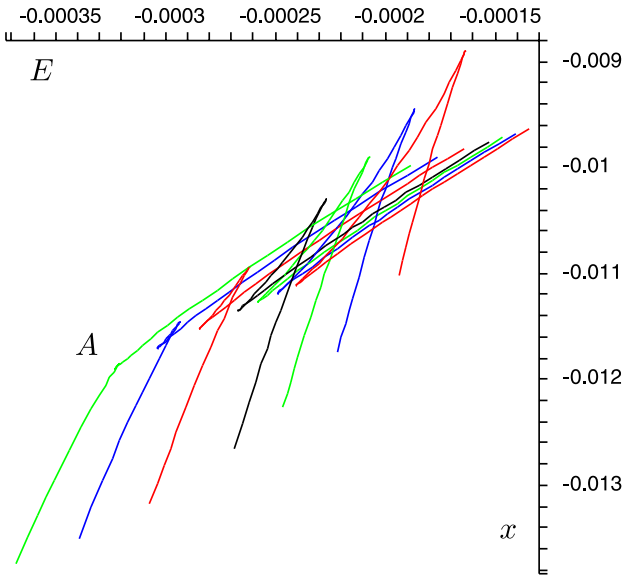

Fig. 11. Sections of energy–momentum space by $\ell^2 = 4 \times 10^{-6}$, $\ell^2 = 5 \times 10^{-6}$, $\ell^2 = 6 \times 10^{-6}$. $\ell^2 = 7 \times 10^{-6}$, $\ell^2 = 9 \times 10^{-6}$, $\ell^2 = 11 \times 10^{-6}$, $\ell^2 = 13 \times 10^{-6}$. Model calculation with $y = 1/10$. (For interpretation of the references to color in this figure legend, the reader is referred to the web version of this paper.)

level and boundary of the reduced space. Fig. 11 shows what happens when we approach these particular ℓ^2 value.

In a similar way we can plot critical values which belong to the $x = \text{const}$ section of the 3D-image of the $\mathcal{EM}$ map. Corresponding sections are shown in Figs. 12 and 13.

If we look at critical lines on the $x = \text{const}$ sections of the image of $\mathcal{EM}$ map, then for negative x sufficiently close to zero we see two disconnected components of the boundary. Remind that we use graphical representation in terms of ℓ rather than of ℓ^2. One boundary is represented by a closed curve. The inverse image of each points inside it corresponds to a regular torus. Another boundary line also separates points which have regular torus as inverse image (to the left of the curve on the figure) and which have not (to the right of the curve). This means that there is region where the complete inverse image of each point of the $\mathcal{EM}$ map has two disconnected regular tori. When x decreases further two boundaries touch each other and we have one self-intersection curve. Again any point inside small triangles possesses two disconnected tori as inverse image. Further decrease of x leads to shrinking of the region of existence of double valued inverse map and to disappearance of singularities on the boundary.

4.3. 3D-image of the $\mathcal{EM}$ map

Now, after looking at different sections of the 3D-image of the $\mathcal{EM}$ map we can go to the complete 3D-representation. At low n (or equivalently at $x < 0$) the 3D-image has very simple form of a 3D-body with one vertex and three singular lines on its 2D-boundary. These singular lines are shown in Fig. 14. At the same time within the scale used in Fig. 14 it is impossible to represent the most interesting region of the 3D-image of the $\mathcal{EM}$ map near $E = x = \ell = 0$ where the subcritical bifurcation leads to the qualitative modification of the image. This small but important region is shown separately in Fig. 15. The importance of this region is due to the presence of a part of $\mathcal{EM}$ image which has two disconnected components of the inverse image of $\mathcal{EM}$ map.

Author's personal

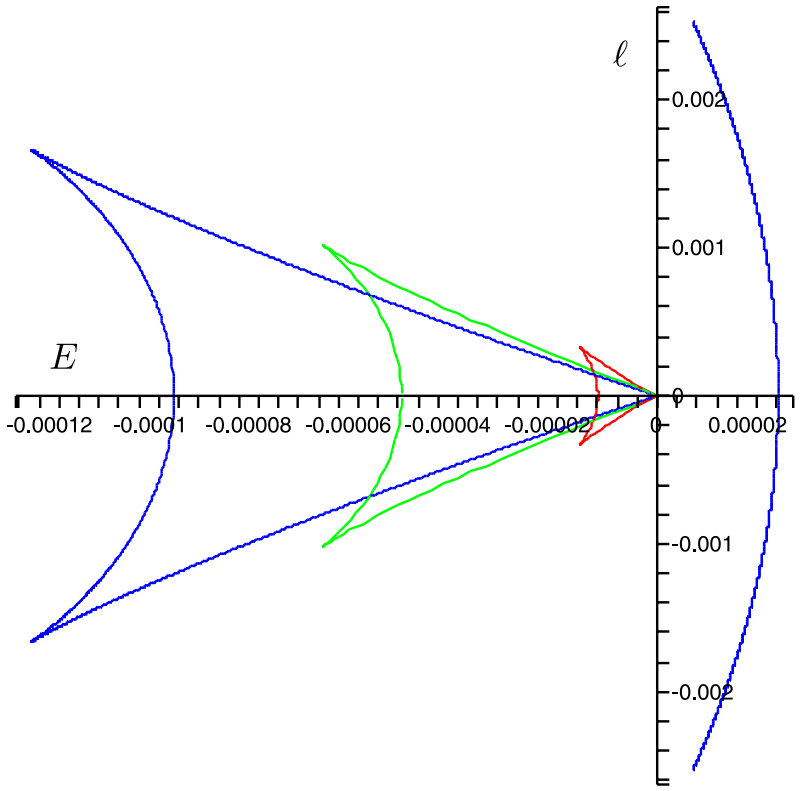

Fig. 12. Sections of energy–momentum space by $x = -0.003$ (red), $x = -0.006$ (green), and $x = -0.008$ (blue). The outside boundary of the image of the $\mathcal{EM}$ map is visible only for $x = -0.008$. For other values of x it is far away in the scale of the figure. Model calculation with $y = 1/10$. (For interpretation of the references to color in this figure legend, the reader is referred to the web version of this paper.)

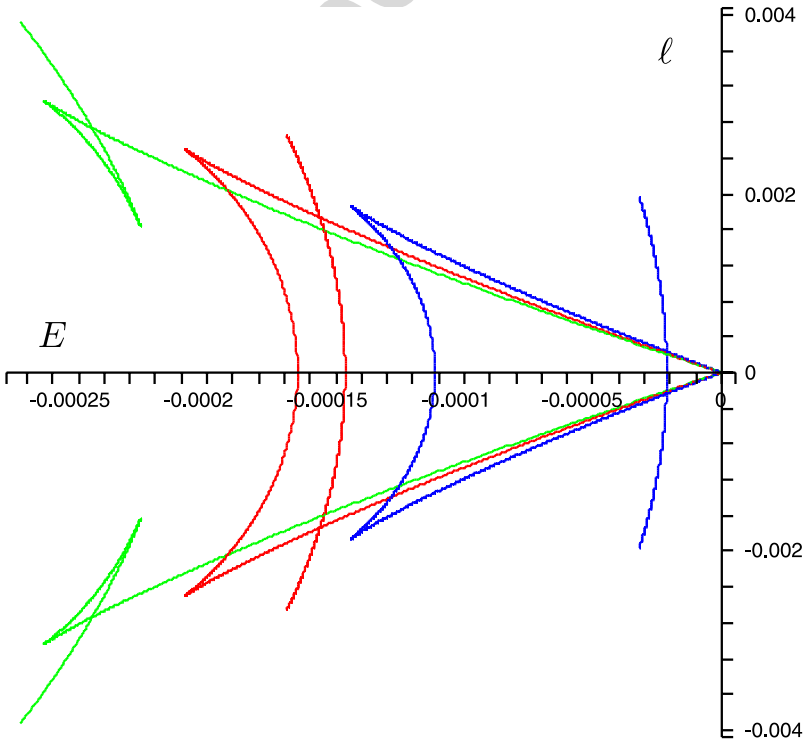

Fig. 13. Sections of energy–momentum space by $x = -0.0085$ (blue), $x = -0.01$ (red), and $x = -0.011$ (green). Model calculation with $y = 1/10$. (For interpretation of the references to color in this figure legend, the reader is referred to the web version of this paper.)

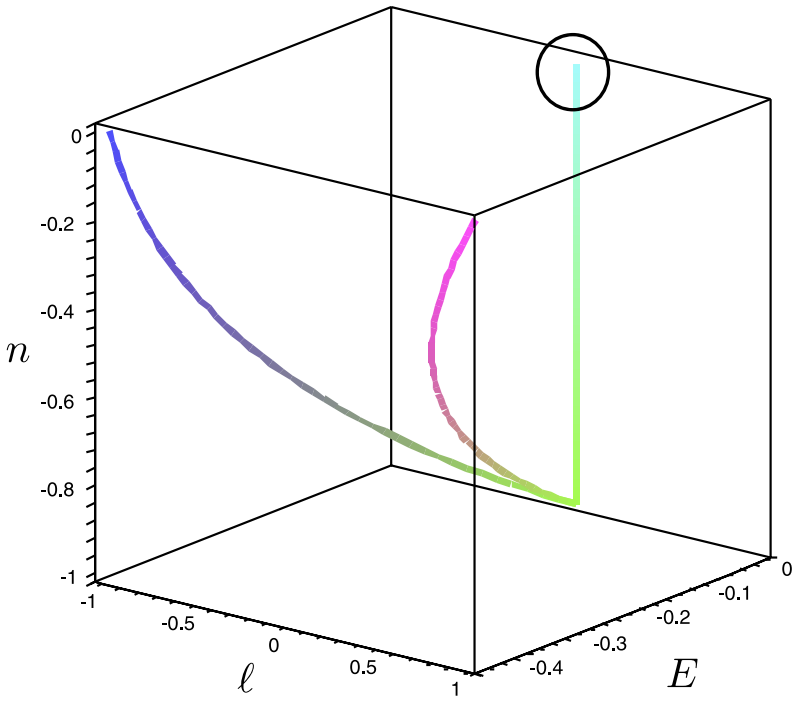

Fig. 14. Singular lines on the boundary of $\mathcal{EM}$ image. Model problem with $y = 1/10$ or $u = (1 + 2/10)^{1/6}$. The detailed representation of the boundary within the region near $E = x = \ell = 0$ indicated by a big circle is given in Fig. 15.

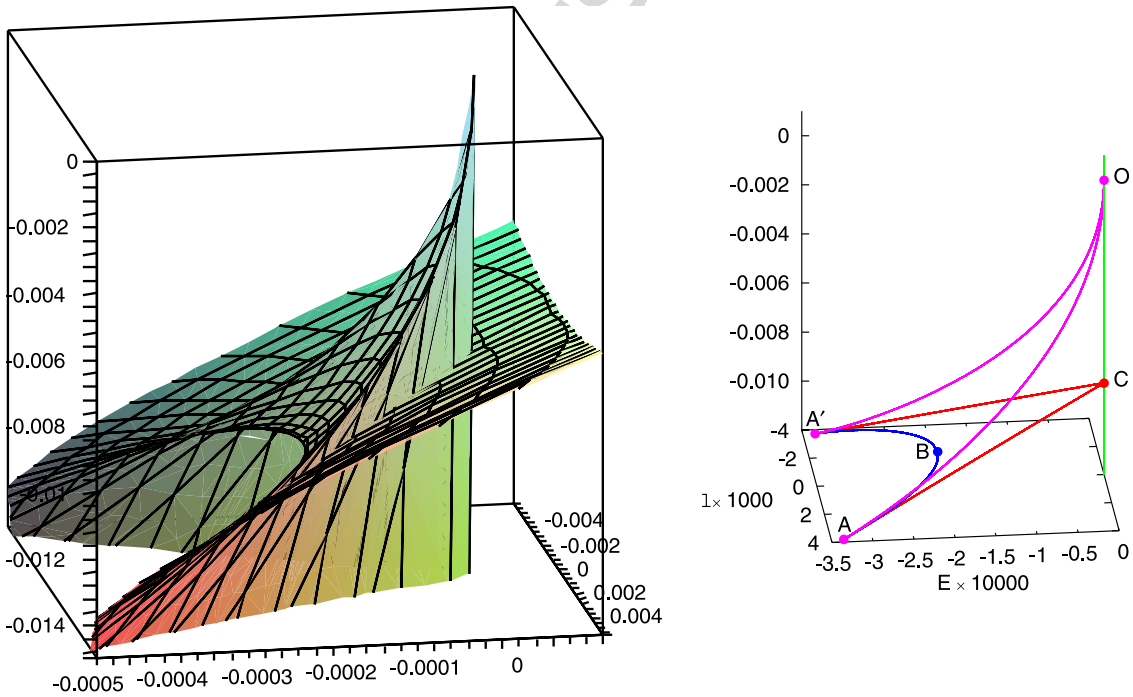

Fig. 15. On the left: Part of the self-overlapping boundary of the 3D-image of the energy–momentum map EM for a model of slightly detuned 1:1:2 resonance described by Eqs. (13a) and (13b) with $y = 1/10$ in coordinates (E, ℓ, x). Regular $\mathcal{EM}$ values lie left and above the boundary. Inverse $\mathcal{EM}$ images of points inside the swallow-tail-like 3D-region have two disconnected components. On the right: Singular lines in the image of the $\mathcal{EM}$ map which give a contour (edges) of the swallow-tail-like region. Values of $\mathcal{EM}$ which correspond to the second order touching of the constant energy level set and the reduced phase space correspond to AO, $A'O$, and ABA' lines; AC and $A'C$ indicate self-intersection of the boundary; OC line corresponds to the main singularity of the 1:1:2 resonance.

Table 1
Coordinates of exceptional points on the image of the $\mathcal{EM}$ map as a function of parameter $u > 0$ and corresponding critical points of the reduced phase space $\{R, S, T = 0\}$

Variable	Point O	Point A	Point B	Point C	Point M
ℓ^2	0	$\frac{4(1-u^3)^4}{(1+u^6)^4}$	0	0	0
E	0	$-\frac{u^{12}-6u^6+8u^3-3}{(1+u^6)^3}$	$-\frac{(u^2-1)^3}{(u^4-u^2+1)^3}$	0	0
x	0	$\frac{-3+4u^3-u^{12}}{(1+u^6)^2}$	$-\frac{(u^4+2)(u^2-1)^2}{(u^4-u^2+1)^2}$	$-\frac{(u^6-1)^2}{(1+u^6)^2}$	-1
R	0	$\frac{2(u^6-1)}{(1+u^6)^2}$	$\frac{2(u^2-1)}{(u^4-u^2+1)^2}$	$\frac{4(u^6-1)}{(1+u^6)^2}$	0
S	0	$\frac{8u^3(u^3-1)}{(1+u^6)^3}$	$\frac{2(u^2-1)}{(u^4-u^2+1)^3}$	$\frac{8(u^6-1)}{(1+u^6)^3}$	0

The region with two components of the inverse image (or two fibers) is characterized by its 2D-boundary, by 1D-singular lines on this boundary and by exceptional points on these lines. Fig. 15, right shows all exceptional points and lines. Below we use the points A, A', B, C, O to label singular lines and 2D-faces of the boundary of the region with two components of the inverse image of $\mathcal{EM}$ map. The coordinates of these exceptional points are listed in Table 1. Derivation of corresponding analytical expressions for 0D-, 1D-, and 2D-strata on the image of $\mathcal{EM}$ map is given in Appendix A.

5. Global analysis of classical system: monodromy and bidromy

Fig. 15, Table 1 and analytical expressions in Appendix A describe the boundary of the image of energy–momentum map for the problem with slightly detuned 1:1:2 resonance and all special points and lines on this boundary.

5.1. Fibers of the $\mathcal{EM}$ map

On the basis of this description we concluded that this classical system has a special feature in the case of parameter u slightly grater than 1, namely the existence of the domain of the regular values in the image of the $\mathcal{EM}$ map where the inverse image of each value consists of two disconnected fibers. We denote this "self-overlapping" region by $OCAA'$ (see Fig. 15). Each regular fiber in the inverse images is a regular three-torus. Let us denote them as T^3_α and T^3_β. One of these tori, say T^3_α degenerates into T^2_α on the internal points of the 2D-boundaries OAC and $OA'C$ while another component remains the T^3_β regular torus at that boundary and can be deformed smoothly along the path crossing this boundary. At the same time the T^3_β torus degenerates into T^2_β at the internal points of the boundary CAA' while T^3_α remains regular three-torus at that boundary and can be deformed smoothly along the path crossing that boundary.

At the internal points of the boundary OAA' the two 3D-tori glue together. At the internal points of the singular lines AC and $A'C$, the inverse image is a disjoint union of two 2D-tori $T^2_\alpha \oplus T^2_\beta$. The lines AC and $A'C$ are formed by the self-intersection of the boundary. Each of the two components of the inverse image $T^2_\alpha \oplus T^2_\beta$ can be associated

Author's personal copy

with a particular degenerate two-torus over the appropriate regular points on the boundary. Such arrangement is a 3D-analog of the situation discussed in the introduction (see Fig. 4). In particular, the line c in Fig. 4 is the analog of the 2D-fragment AOA' of the boundary in Fig. 16. The line c in Fig. 4 is formed by values of $\mathcal{EM}$ map whose inverse images are 2D-bitori. The 2D-fragment AOA' of the boundary in Fig. 16 is formed by values of 3D $\mathcal{EM}$ map whose inverse images are 3D-bitori.

5.2. "Really closed" and "virtually closed" paths in the (E, x, ℓ) space

Let us discuss now the deformation of the regular tori as their $\mathcal{EM}$ images move along different paths in the (E, x, ℓ) space. We suppose that the path starts at some regular point t_0 inside the self-overlapping region. We need to distinguish connected components which we denote as (t_0, α) or (t_0, β) and to associate with path one of these components. If the path remains inside the self-overlapping region in the (E, x, ℓ) space and forms a closed loop, i.e. it returns back to the point t_0, the connected component cannot change along this path. In such a case the same connected component is associated with the initial and the final points of this closed path in (E, x, ℓ) space. We call such path together with associated continued family of tori the *really closed* path. We can easily generalize this notion to paths which can leave the self-overlapping region of the (E, x, ℓ) space. The only requirement which should be imposed on the path and the associated component is: the initial and the final points of the "really closed" path are associated with the same component. It is clear that in the case when "really closed" path does not leave the self overlapping region it is homotopic to a point. Generically "really closed" paths can be homotopically non-equivalent due to the presence of the singular thread on the image of the $\mathcal{EM}$ map.

Along with "really closed" paths another class of closed paths can be constructed. We will name these paths "virtually closed". In order to construct an example of such path we need to take into account that one of two components present in the self-overlapping

personal copy

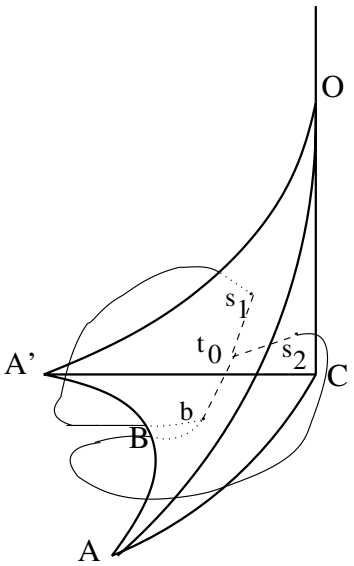

Fig. 16. Region of the image of EM map whose points have two connected components in their inverse images. Two homotopically inequivalent paths $(t_0^{(1)} - b - s_2 - t_0^{(2)})$ and $(t_0^{(1)} - b - s_1 - t_0^{(2)})$ are shown. Their difference, i.e. the path $(t_0^{(1)} - b - s_2 - t_0^{(2)} - s_1 - b - t_0^{(1)})$ is equivalent to a closed path surrounding once the singular line $O\infty$. Points s_1,s_2,b are located on the boundaries $s_1 \in A'CO$, $s_2 \in ACO$, $b \in AA'C$, point t_0 is inside the 3D-body.

region, for example the T^3_α component, can be deformed smoothly out of this region as the associated path crosses the boundary $AA'C$. Another, T^3_β, connected component degenerates at this boundary. At the same time the T^3_β component can be deformed smoothly out of self-overlapping region as the associated path crosses the boundaries OAC or $OA'C$ including the line OC. Only T^3_α component degenerates at this boundary. But neither OAC and $OA'C$ boundaries nor singular line OC are special for T^3_β component. Note further that neither component can be smoothly deformed through the boundary OAA' where fusion of two components takes place.

It is quite clear that the path starting at an initial point t_0 and going out of self-overlapping region can come back to the self-overlapping region either by passing through the same boundary or across another boundary. Coming back through the same boundary we return to the same connected component. Coming back to point t_0 results in such a case in getting "really closed" path. If we return back to the initial point t_0 through another boundary we come to the alternative component. The so obtained path has the same initial and final point t_0 in the (E, x, ℓ) space, but the initial and the final components are different. Although this path seems to be closed in the (E, x, ℓ) space, the associated components at initial and final points are different. We name such paths "virtually closed".

Among all "really closed" and "virtually closed" paths there are homotopically non-equivalent paths. This follows from existence of the singular line $O\infty$ which is equally present for 1:1:2 resonant problem without detuning.

In order to construct homotopically non-equivalent paths it is sufficient to make different number of circles around singular line $O\infty$ after the path goes out of the self-overlapping region and before it returns back to the initial point t_0. The simplest example of two non-equivalent "virtually closed" paths can be easily constructed (see Fig. 16). Let us begin at an internal point t_0 of the self-intersection region. We take one path which goes out of this region through point b in the "bottom" and then return back by going above the OA singular double touching line and by entering inside the self-overlapping region through point s_2 on the "side boundary" OAC. Another path goes out of the self-overlapping region through the same point b but after that goes above the OA' singular line and enters inside by passing through the point s_1 on the "side boundary" $OA'C$. Obviously, these two paths are "virtually closed" because initial and final components are different and they are not homotopy equivalent. Their difference is equivalent to the closed path surrounding once the singular line 0∞. The proof of this statement is quite simple. Let us consider the closed path representing the difference of two initial paths. This path starts at point t_0 on component α. Then it goes through points b and s_2 to t_0^β and continues further through s_1 and b to t_0^α. It is clear that the part $s_2 - t_0^\beta - s_1$ of this path can be smoothly deformed out of two component region because all points of this part belong to β component which does not "notice" the boundaries ACO, $A'CO$ and line OC. In a similar way the part $b - t_0^\alpha - b$ can be smoothly deformed out of the two-component region. The resulting closed path represents just a closed loop around the singular line $O\infty$.

5.3. Bipath and crossing the bitorus boundary

As soon as we have established the correspondence between the regular tori at both sides of the "unpenetrable" boundary OAA', we can try to define the correspondence between the regular tori in the neighborhood of this boundary at which the two tori glue together. This enables us to define a procedure of crossing such boundary.

Author's personal copy

The first step consists in generalizing the notion of a path associated with one component. When crossing "bitorus" boundary we leave the region of the (E,x,ℓ) space with one component and enter the region of the (E,x,ℓ) space with two components for each value (E,x,ℓ). Thus we allow for a single path to bifurcate at the boundary, i.e. to transform one path in (E,x,ℓ) space associated with single fiber into two paths associated each with its own components. We consider these two paths as two components of the same *bipath*. These two components of the bipath are in some way independent and can be different in the (E,x,ℓ) space. To construct the closed bipath we need to introduce a new operation which enable us to joint the two components into one on a regular fiber of the $\mathcal{EM}$ map. The schematic representation of the bipath is given in Fig. 17 where in order to simplify the representation we use the 2D-image of the $\mathcal{EM}$ map in (E,m) coordinates. In this Fig. 17 the regular values of the $\mathcal{EM}$ map having one component as inverse image are shown by light shading, while regular values possessing two disconnected fibers in the inverse image are shown by dark shading (MNO region). Singular line MN corresponds to bitorus in the inverse image. Line NO corresponds to degeneration and disappearance of one component, while another component degenerates and disappears at line MO. Closed bipath starts end ends at point A. At point B lying on the bitorus line it splits into two components associated with different fibers. These two components of the bipath go out of the two-fiber regions through different boundaries (points e and f). Further, two components of the bipath go to the same regular point D where they fuse into one path joining the initial point A.

5.4. Evolution of cycle bases along bipath and bidromy transformation

Now we need to define the evolution of the basis of cycles of regular tori (basis of the first homology group) along a so constructed bipath. There are two points which require special attention. Point corresponding to crossing of the bitorus line (point B in Fig. 17) and point, where the fusion of two components takes place (point D in Fig. 17). In order to allow the reasonable evolution of the basis cycles when crossing the bitorus line, we suppose that one cycle g_m is globally defined because it is related with the globally defined action (geometrical or dynamical symmetry). As another cycle we take double cycle $2g_e$ which forms figure eight on the bitorus line. When the bipath splits into two components, the associated double cycle transforms into two single cycles for two separate components

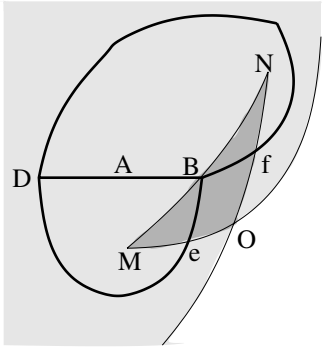

Fig. 17. Construction of a closed bipath with point A as initial and final point. Point B is the point of bifurcation into two components BeD and BfD. Point D is the point of fusion of two components into one path DA. Light shading corresponds to regular values of the $\mathcal{EM}$ map with one component in the inverse image. Dark shading corresponds to regular values of the $\mathcal{EM}$ map with two disconnected components.

Personal copy

$2g_e = g'_e + g''_e$. Thus, after returning to the point of fusion D the two components have cycle bases (g_m, g'_e) and (g_m, g''_e). These two sets of cycle bases have one common cycle. Now the fusion of two components of a bipath into one corresponds at the level of cycle basis to the following transformation:

$$(g_m, g'_e) \oplus (g_m, g''_e) = (g_m, g'_e + g''_e). \tag{16}$$

The transformation between the initial cycle basis and the final cycle basis gives the bidromy transformation associated with the chosen bipath. In fact this transformation was introduced only for some subgroup of the first homology group, but as soon as the initial (and the final) point is a regular one we can easily extend the transformation to the complete homology group. This transformation is unimodular, but it may has fractional coefficients.

Extension of the discussed above bipath construction and bidromy transformation to our initial 3D-problem is straightforward. We choose the basis of the homology group of regular torus $\{g_1, g_2, g_3\}$ in the one-component-region in such a way that after a deformation of this basis along a path in the $\{E, n, \ell\}$ space till the critical value associated with the bitorus, one of the basis cycles, say g_3, becomes figure eight and splits into two cycles after the path enters the two-component-region and bifurcates into the two-component bipath. At the same time two other basis cycles $\{g_1, g_2\}$ deform smoothly because they are related to two actions, n, ℓ. Remind that ℓ is the global action because it is due to global geometrical symmetry. Another integral of motion, n, is also a global action due to construction of the integrable model by the normalization.

As soon as splitting of one basis cycle into two is not a well defined procedure we choose as the initial basis in the one-component region the basis of the subgroup of the homology group which has the form $\{g_1, g_2, 2g_3\}$. The so chosen system of cycles forms the basis of the index 2 subgroup of the homology group of regular tori in the one-component region. After crossing the line of critical values, i.e. passing through the bitorus line the system of basis cycles $\{g_1, g_2, 2g_3\}$ transforms into two systems of basis cycles for two regular tori $\{g_1, g_2, g'_3\}_{b'}$ and $\{g_1, g_2, g''_3\}_{b''}$ associated with two component of a bipath which have appeared after a bifurcation of the initial path at the bitorus line. Now for each fiber (i.e. for each of the two connected components of the inverse image of the $\mathcal{EM}$ map) the indicated system of cycles forms a basis of the whole homology group.

Further deformation of the two cycle bases can be done independently along two different components of the bipaths but we follow the evolution of two bases along these different components together. Each component of the bipath goes only through regular tori. But within the two-component region these two tori belong to different fibers and, consequently in order to leave the two-component region one component of the bipath should go out through the "side boundary" (AOC or $A'OC$ on Fig. 15, right) while another component of the bipath should go out through the "bottom boundary" (ACA' on Fig. 15, right). Both components of the bipaths return to the initial point. Now the basis of the same homology group of the same regular torus is associated with each component of the bipath. These two bases are not necessarily identical because they are associated with paths which are not homotopically equivalent. Moreover, these two bases are generically different from the initial basis $\{g_1, g_2, g_3\}$ of the homology group of the initial regular torus. The simplifying fact which we can use when writing explicitly the final bases to both paths is the persistence of the cycles associated with the two global actions, n, ℓ. Only the third basis element can vary when returning back to the initial point. Let us denote the two bases associated with the same regular torus at the end of the two components of the

Author's personal copy

bipaths as $\{g_1, g_2, g_3^s\}$ and $\{g_1, g_2, g_3^b\}$. Here the g_3^s cycle is the third basis element of the homology group of the regular torus deformed along a component of the bipath going out of two-component region through the "side" boundary. The g_3^b cycle is the third basis element of the homology group of the regular torus deformed along a component of the bipath going out of two-component region through the "bottom" boundary.

Now in order to compare the two bases $\{g_1, g_2, g_3^s\}$ and $\{g_1, g_2, g_3^b\}$ of the homology group of the final regular fiber in the one-component region with the basis $\{g_1, g_2, 2g_3\}$ of the subgroup of the homology group chosen at the initial point we need to "fuse" two bases into one. This procedure should be in some sense reciprocal with respect to splitting of the basis into two bases when passing the singular bitorus. We suggest to define the "fusion" of two bases as the operation which gives instead of two bases $\{g_1, g_2, g_3^s\}$ and $\{g_1, g_2, g_3^b\}$ of the full homology group of the regular torus, the basis of an index two subgroup $\{g_1, g_2, g_3^s + g_3^b\}$ of the homology group of the same regular torus.

Finally, we can compare the initial basis $\{g_1, g_2, 2g_3\}$ with the final basis $\{g_1, g_2, g_3^s + g_3^b\}$. Both these bases are defined for regular tori which belong to one-component region of the image of the $\mathcal{EM}$ map. This allows us to define the transformation of the system of cycles of the regular torus induced by the deformation along the bipath as "*bidromy*" transformation.

The initial and the final bases are bases for subgroups of the same homology group and consequently these bases can be expressed as combinations with integer coefficients of basis cycles of the full homology group of the regular torus. The determinant of the matrix of transformation from the basis of the group to the basis of the subgroup equals the index of the subgroup, i.e. two in our case. At the same time, the matrix of transformation between initial and final bases has determinant 1, but generically it has fractional coefficients. We call this matrix the *bidromy* matrix associated with the "bidromy" transformation. The bidromy characterizes the transformation of the "passable basis" of cycles of a regular torus associated with a "bipath" which crosses the line of critical values representing bitorus.

We note that we introduced the new operation of "splitting" and "fusion" of bases of homology groups to define the bidromy. In our particular case this operation relates the basis of the subgroup of index 2 of the homology group of regular torus with two bases of the total homology group. We formally write this operation as:

$$\{g_1, g_2, g_a + g_b\} \leftrightarrow \{g_1, g_2, g_a\} \oplus \{g_1, g_2, g_b\} \tag{17}$$

This operation can be done for a regular torus and for a special kind of a singular torus, the bitorus. Applying this operation to bitorus is associated with the bifurcation of the single path into two components of the bipaths. The reason for introducing such operation is intuitively clear. It is necessary to generalize the notion of monodromy to more complicated situations, when the path crosses the boundary separating regions of critical values with one-component and two-component inverse images of the $\mathcal{EM}$ map. We do not discuss in this paper a rigorous mathematical definition of this operation and of the related concept of "bidromy". Instead, in the next section we demonstrate very appealing manifestations of bidromy in one corresponding quantum problem.

6. Quantum monodromy and quantum bidromy

We now describe how such specific structure of classical toric fibration as "bidromy" manifests itself in the joint energy–momentum eigenvalue spectrum of the corresponding

Author's personal copy

quantum problem. In order to simplify the analysis, let us restrict the system to $\ell = 0$ and consider the respective section of the image of the $\mathcal{EM}$ map together with the quantum lattice as shown in Fig. 18. The lattice in Fig. 18 is computed for the Hamiltonian (13a) and (13b) with $\hbar = 0.0002$ and $N = 4910, \ldots, 5010$, where $\hbar N = n = 1 - x$. In this $\ell = 0$ section, the two component region forms the 2D domain *BCO*. Our analysis of the classical system suggests that the joint quantum energy–momentum spectrum can be unfolded as a regular $\mathbb{Z}^2$ lattice which self-overlaps in the region *BCO*. In this latter region we have two sublattices which correspond to two fibers in the inverse image of classical $\mathcal{EM}$ map. Indeed these sublattices can be seen clearly in Fig. 18, and we can also see that one of the sublattices can be continued smoothly out of the self-overlapping region *BCO* through its right side boundary *CO*, whereas the other sublattice continues smoothly through the bottom boundary *BC*. Far outside *BCO* the two sublattices join smoothly and become one lattice. It follows that all quantum states represented by the lattice in Fig. 18 can be assigned using one system of global quantum numbers. However, states with close energy–momentum and polyad characteristics in the overlap region *BCO* can have very different quantum numbers if they belong to different sublattices.

The lattice in Fig. 18 stimulates another more complicated conjecture on the possibility to transfer a quantum cell across the merger line *BO* (a singular line at which the preimage of the classical $\mathcal{EM}$ value splits into a pair of regular tori). This quantum construction replicates essentially the classical "bidromy" transformation introduced in the previous section.

We begin with a double cell which splits into two cells after crossing the merger line *BO*. The new cells belong to two different sublattices. At the same time, the path along which we follow the evolution of the cells splits into two: one goes up around vertex *O* and the other follows down and turns around *B*. In fact, instead of a standard path we have the more complicated construction of "bipath". The "bipath" is characterized by a bifurcation point where the single path splits into two components of bipath. Each of the two cells is now designated to its own path (or more exactly to its component of the "bipath"), and we should follow their evolution simultaneously. After our cells return back (each along its own component of "bipath"), the two branches of "bipath" fuse together forming a single path where the resulting cells can be arranged as shown in Fig. 18, i.e. by having one common side. After that we need a quantum analog of the "fusion" operation to fuse them into a single double cell and to compare the latter to the initial double cell. The transformation between the initial and final double cells defines the quantum *bidromy* matrix. In particular, the "bidromy" transformation between the initial and final cells for the example shown in Fig. 18 can be written in the matrix form as:

$$\begin{pmatrix} \frac{1}{2} & 0 \\ 1 & 2 \end{pmatrix}. \tag{18}$$

The appearance of $\frac{1}{2}$ in (18) is the consequence of the fact that only cells doubled in the "*E*-direction" can follow the bipath and cross the singular line *OB*. At the moment of crossing the bipath bifurcates and the cell splits into two cells in such a way that the total volume of two cells remains equal to the volume of the initial double cell. The same conservation of volume takes place at the moment of the second bifurcation associated with the fusion of the two components of "bipath" into a single path, where we reconstruct the single cell from the two cells arriving from two branches of the "bipath". The conservation of volume manifests itself as the requirement that the determinant of the bidromy matrix is 1.

Author's personal copy

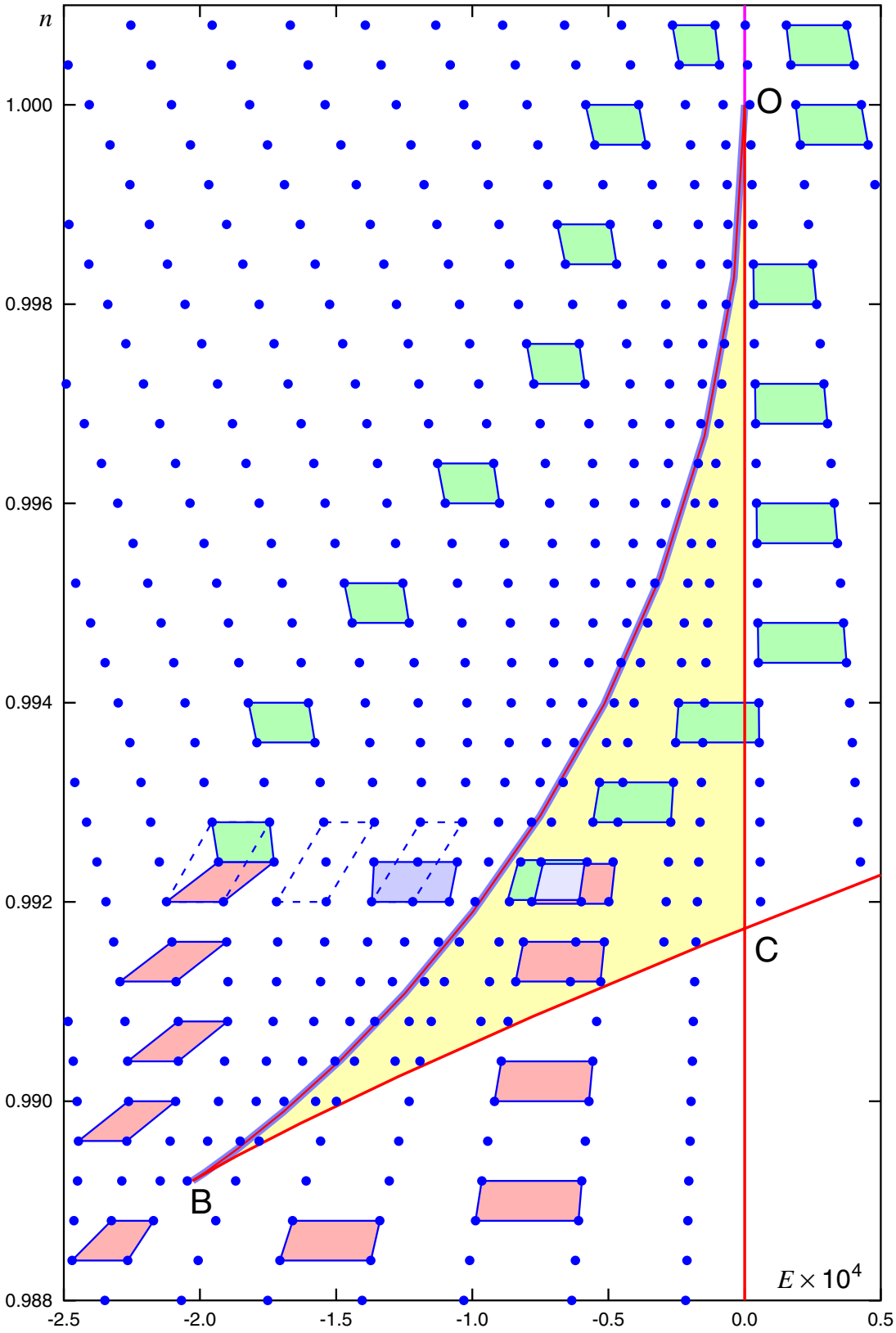

Fig. 18. Quantum spectrum (blue dots) of a slightly detuned 1:1:2 resonant oscillator (given by Eqs. (13a) and (13b) and $y = 1/10$) with $\ell = 0$ in the (E,n) region corresponding to the existence of two classical fibers. Values of $h = 0.0002$ and $N = 4910,\ldots,5010$ are used in quantum calculations, where $hN = n = 1 - x$. Elementary cells represent a tentative interpretation of bidromy in terms of cell transportation admitting splitting and fusion of cells at the branching points of the bipath. (For interpretation of the references to color in this figure legend, the reader is referred to the web version of this paper.)

Certainly, in order to justify such construction, the operation of splitting and fusion of quantum cells associated with bifurcations of "bipath" should be mathematically approved. The invariance of the "bidromy" transformation on the choice of the "bipath" should also be proven. We leave these questions open. We point out only to the fact that for the analyzed example, new qualitative characteristics of the pattern formed by the joint spectrum lattice are introduced naturally and are described in a rather simple and visualized form.

7. Conclusions

We like to comment that 1:1:2 resonant molecular systems with bidromy are not very likely to exist among known molecular systems with Fermi resonance. Thus all such systems we know undergo the supercritical bifurcation. In CO_2, where detuning b is anomalously small, this bifurcation occurs for n well below the value $n = \frac{3}{2}$ of the ground state; in CS_2 it happens at the level of the first overtone. However, the Fermi resonance and the three degrees of freedom are by no means necessary for the system to have bidromy. It is also possible to observe this phenomenon in systems with two degrees of freedom [36] and resonance 1:1.

Naturally, a generalization of the bidromy notion to "multidromy" can be done in a quite straightforward way in the case of problems with more complicated singularities associated with splitting or fusion of several tori [32]. One of such appealing more complicated concrete problems is the Manakov top. But ever before going to such complications, there are a lot of more simple questions to analyze and to justify especially from the point of view of mathematically rigorous foundation. So the most important and urgent next step is to construct the simplest, in some sense "elementary" or universal model problem with bidromy using as example the dynamical system with two degrees of freedom only [37].

Appendix A. Critical values of the energy–momentum map

In this appendix, we give the details of the analytical derivation of equations describing critical values of the $\mathcal{EM}$ map for the integrable 3D-system of the 1:1:2 resonant oscillator with detuning studied in the main text. This analysis is based on the study of the system of Eqs. (13a,13b) describing the relative position of the constant energy level set of the Hamiltonian and the boundary of the reduced phase space.

A.1. $\ell = 0$ case

In order to illustrate our approach we start this analysis with one particularly simple case, corresponding to $\ell = 0$. In such a case (13a,13b) in u parameterization takes the following form:

$$H = S - R + \frac{u^6 + 1}{4} R^2; \tag{A.1a}$$

$$S^2 = R^2(1 + x - R). \tag{A.1b}$$

One obvious critical point of the $\mathcal{EM}$ map corresponds to $R = S = 0$. It is due to the singularity of the reduced phase space for $\ell = 0$. In order to find other critical points of the

Author's personal copy

$\mathcal{EM}$ map we need to find the R, S values at which the energy level defined by (A.1a) touches the boundary defined by (A.1b). The mathematical condition for such touching is:

$$\frac{\partial S^{\mathrm{En.L}}}{\partial R} = \frac{\partial S^{\mathrm{b}}}{\partial R}, \tag{A.2}$$

where $S^{\mathrm{En.L}}$ is the expression for S found from energy level Equation (A.1a) and S^{b} is the S expression found from the boundary Equation (A.1b). After calculating derivatives,

$$\frac{\partial S^{\mathrm{En.L}}}{\partial R} = \frac{\partial}{\partial R}\left[E + R - \frac{u^6+1}{4}R^2\right], \tag{A.3}$$

$$\frac{\partial S^{\mathrm{b}}}{\partial R} = \frac{1}{2S}\frac{\partial}{\partial R}\left[R^2(1+x-R)\right], \tag{A.4}$$

we need to use once more the boundary equation (A.1b) in order to eliminate S from the resulting equation and to get the polynomial equation

$$\begin{aligned}&(u^6+1)^2R^3 + (-u^{12} - 6u^6 + 4 - xu^{12} - 2xu^6 - x)R^2\\ &\quad + (-4 - 8x + 4xu^6 + 4u^6)R + 4x + 4x^2 = 0,\end{aligned} \tag{A.5}$$

which gives the positions of touching points between energy levels and the boundary for given values of integral x and of parameter u. This equation is cubic in R and quadratic in x. It is also polynomial (of degree 12) in u. Two solutions for $x(R,u)$ as a function of R and of parameter u can be used to construct the parametric representation $E(R,S(R,x(R)))$, $x(R)$ of the critical values on the image of $\mathcal{EM}$ map, i.e. in the plane (E,x), using R as parameter. For these two solutions $x_{1,2}(R;u)$ we have

$$\begin{aligned}x_{1,2}(R;u) = {}&\tfrac{1}{8}R^2(u^6+1)^2 + R - \tfrac{1}{2}Ru^6 - \tfrac{1}{2} \pm \tfrac{1}{8}\big(16 - 32Ru^6 + 8R^2(3u^{12} + 2u^6 - 1)\\ &-8R^3u^6(1+u^6)^2 + R^4(1+u^6)^4\big)^{1/2}.\end{aligned} \tag{A.6}$$

We can easily distinguish these two solutions through their behavior at $R = 0$. The solution which go to 0 as $R \to 0$ describes the appearance of new critical points for x close to 0. Another solution, which goes to $x = -1$ for $R \to 0$ describes the boundary near the equilibrium point.

These two solutions can become degenerate if the discriminant of the quadratic in x equation becomes zero. Expressing R as a function of u for these degeneracy points we find that only the doubly degenerate solution

$$R_{\mathrm{degen}} = \frac{2}{u^6+1}, \quad \frac{2}{u^6+1}, \tag{A.7}$$

is relevant.

This means that when we construct parametric representation of $E(R)$, $x(R)$ we should be accurate passing the point $R = 2/(u^6+1)$, where two solutions for $x_{1,2}(R,u)$ degenerate.

We can now look at Eq. (A.5) as on the cubic equation in R. When two solutions of this cubic equation become degenerate the discriminant of this cubic equation becomes zero and at the touching point between energy level and the boundary both the first and the second derivatives coincide.

Putting discriminant of cubic in R equation equal to zero gives equation of degree 5 in x which can be factorized and completely solved. The equation itself has the form:

Author's personal copy

$$16(xu^8 - 2xu^6 + 3xu^4 - 2xu^2 + x + 2 - 4u^2 + 3u^4 - 2u^6 + u^8)$$
$$\times (4 + 7xu^4 + 2u^{16}x + u^{16}x^2 + 4x + 6xu^6 + 2u^{14} + u^{16} + 8u^2$$
$$+ 4u^6 + x^2 + 2xu^{12} + u^{12} - u^8 + 3xu^8 + 4xu^{14} + 2x^2u^{14} + 4x^2u^8$$
$$+ 10u^4 + x^2u^4 + 2x^2u^2 + 2x^2u^6 - 2u^{10} + 2u^{10}x^2 + u^{12}x^2 + 8xu^2)$$
$$\times (u^6 - 2 + xu^6 + x)^2 = 0. \tag{A.8}$$

Among all five solutions,

$$X_{1,2} = \frac{2 - u^6}{(u^2 + 1)(u^4 - u^2 + 1)},$$
$$X_3 = -\frac{(u^4 + 2)(u^2 - 1)^2}{(u^4 - u^2 + 1)^2}, \tag{A.9}$$
$$X_{4,5} = -\frac{2u^{12} + 3u^4 + 4 \pm i6\sqrt{3}u^4}{4(u^4 - u^2 + 1)^2(u^2 + 1)^2},$$

the solutions $X_{4,5}$ are irrelevant, because they are complex except at $u = 0$, but at $u = 0$ they correspond to $X_{4,5} = -2$ which is impossible for the initial model with $x \geqslant -1$. The physically interesting one is the following solution

$$X_B = -\frac{(u^4 + 2)(u^2 - 1)^2}{(u^4 - u^2 + 1)^2}, \tag{A.10}$$

which gives the value of $x = X_B$ at which two new branches of critical points appear. This point is denoted as point B in Fig. 8.

The corresponding value of $R = R_B$ at the extremal x value follows from equation for touching points (A.5) by substituting in this equation x by the X_B value. The equation takes the form:

$$(R + 2 - 4u^2 + u^4 + 2Ru^6 - 2u^6 + Ru^{12})(Ru^8 - 2Ru^6 + 3Ru^4 - 2Ru^2 - 2u^2 + R + 2)^2 = 0. \tag{A.11}$$

There are two solutions, but only one is relevant. We can choose the needed solution by imposing requirement that the first derivative by R of the equation for touching points (A.5) should be also fulfilled at the same point. This follows from the fact that at points where the discriminant is zero, the polynomial and its first derivative have the same root. In other words the discriminant of a polynomial is proportional to the resultant of this polynomial and its derivative.

$$3(u^6 + 1)^2R^2 + (-2u^{12} - 12u^6 + 8 - 2xu^{12} - 4xu^6 - 2x)R - 4 - 8x + 4xu^6 + 4u^6 = 0. \tag{A.12}$$

Substituting into Eq. (A.12) X_B from Eq. (A.10) we transform this equation into the product of two factors

$$(Ru^{12} - 2u^6 + 2Ru^6 - 2u^2 + R + 2)(Ru^8 - 2Ru^6 + 3Ru^4 - 2Ru^2 - 2u^2 + R + 2)^2 = 0. \tag{A.13}$$

The common factor for (A.13) and (A.11) gives the needed solution which is:

Author's personal copy

$$R_B = \frac{2(u^2-1)}{(u^4-u^2+1)^2}. \tag{A.14}$$

Now using (A.10) and (A.14) we calculate values of S and of energy at the extremal point.

$$S_B = \frac{2(u^2-1)}{(u^4-u^2+1)^3}, \tag{A.15}$$

$$E_B = -\frac{(u^2-1)^3}{(u^4-u^2+1)^3}. \tag{A.16}$$

Note that the choice of the parametric representation should be checked if the region of R values includes value corresponding to degeneration of two solutions. We illustrate the possible error in improper continuation of the parametric solution over the zero of the discriminant in Fig. A.1.

In order to characterize the region of (E,x) plane where two disconnected fibers exist we need to precise the position of the point where critical line intersects $E=0$ axis (point C in Fig. 8). The position of this point satisfies the following system of equations:

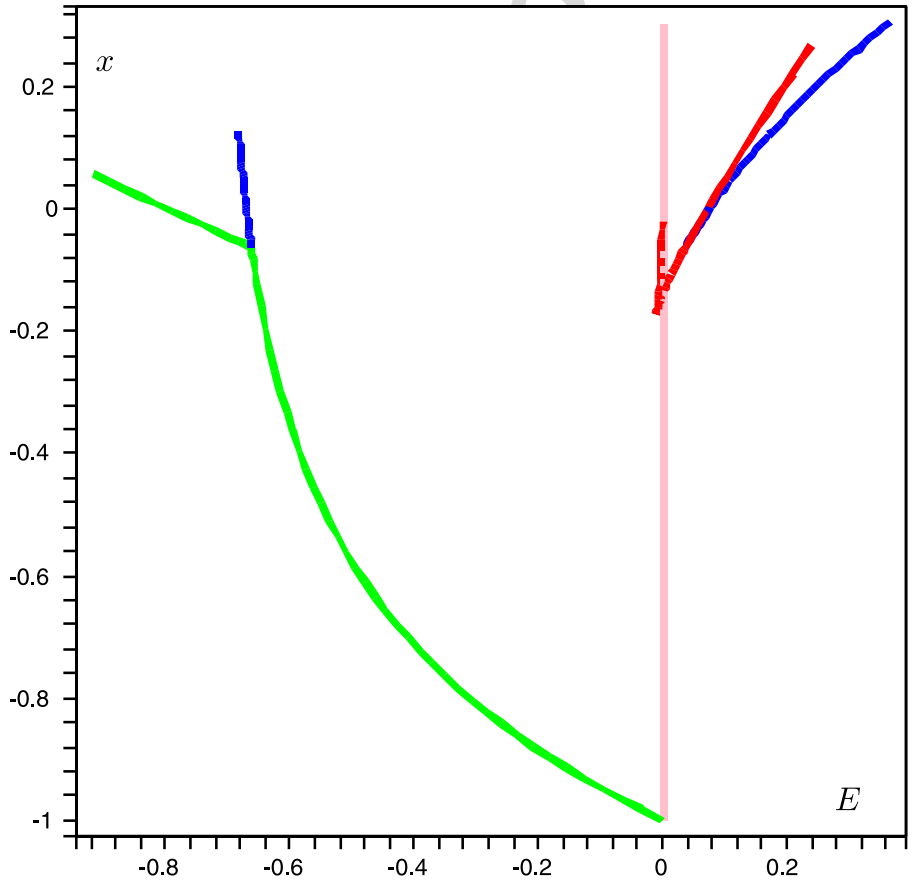

Fig. A.1. Singular values of the energy-momentum map for $\ell^2=0$. Model calculation with $y=3/5$ or $u=(1+6/5)^{1/6}$. Degeneration of two $X_{1,2}$ solutions takes place for such u at $R=5/8$. This figure illustrates the effect of improper continuation of the parametric representation through the point of the zero discriminant. Blue lines should be used to continuer the red and the green lines chosen at small R. (For interpretation of the references to color in this figure legend, the reader is referred to the web version of this paper.)

$$S = R(1 - (u^6 + 1)R/4), \tag{A.17}$$

$$S^2 = R^2(1 + x - R), \tag{A.18}$$

$$S(R(1 + u^6) - 2) = R(3R - 2x - 2). \tag{A.19}$$

Here (A.17) is the equation for energy level with $E = 0$, (A.18) is the equation for the boundary of the "reduced phase space", and (A.19) is the equation specifying that the energy level and the boundary are tangent.

Putting (A.17) into (A.18) and (A.19) we get apart from obvious solution ($R = 0$, $S = 0$) valid for any values of x the system of equations on R and x:

$$x = \frac{1 - u^6}{2}R + \frac{(1 + u^6)^2}{16}R^2, \tag{A.20}$$

$$2x + \frac{3(u^6 - 1)}{2}R - \frac{(1 + u^6)^2}{4}R^2 = 0. \tag{A.21}$$

The nontrivial solution giving the coordinates of point C is

$$R_C = \frac{4(u^6 - 1)}{(1 + u^6)^2}; \quad X_C = -\frac{(u^6 - 1)^2}{(1 + u^6)^2}. \tag{A.22}$$

The corresponding value of S is

$$S_C = \frac{8(u^6 - 1)}{(1 + u^6)^3}. \tag{A.23}$$

We remind that on the image of the $\mathcal{EM}$ map this point (point C) has $E_C = 0$ and $\ell_C = 0$ coordinates.

As a function of u, the so obtained R value has a maximum at $u^6 = 3$. This means that for $u^6 = 3$ the distance between zero singular point and point where the new local solution appears is maximal in R. For $u^6 = 3$ the position of the extremal point (point B) of the energy momentum diagram is

$$E_B(u^6 = 3) = -\frac{(u^2 - 1)^3}{(u^4 - u^2 + 1)^3} \approx -0.019687, \tag{A.24}$$

$$X_B(u^6 = 3) = -\frac{(u^4 + 2)(u^4 - 1)^2}{(u^6 + 1)^2} \approx -0.2974. \tag{A.25}$$

The position of the extremal point is in fact not far from the point of intersection with singular line. Moreover, the extremal energy as a function of u has minimum at $u = \sqrt{2}$.

A.2. $\ell \neq 0$ case

In the case of arbitrary nonzero ℓ the initial system of Eqs. (15a, 15b) can be easily rewritten in the form of equation on the touching points between the energy level and the reduced phase space boundary as it was done earlier in the $\ell = 0$ case. But now instead of the Eq. (A.5) obtained in the case of $\ell = 0$, similar equation for arbitrary ℓ has more complicated form

Author's personal copy

$$(u^6+1)^2R^5+(4-u^{12}-xu^{12}-6u^6-2xu^6-x)R^4+(-8x+4xu^6-2\ell^2u^6-\ell^2 -\ell^2u^{12}-4+4u^6)R^3+(4x^2+\ell^2x+\ell^2xu^{12}+2\ell^2xu^6+4x+6\ell^2u^6-\ell^2+\ell^2u^{12})R^2 -4\ell^2(1+xu^6+u^6)R+\ell^2(\ell^2+4x+4)=0. \quad (A.26)$$

This equation is of degree 5 in R but only quadratic in x and in ℓ^2. This means that we can find for fixed ℓ^2 value the relation between x and R by solving quadratic equation and find for fixed x values the relation between ℓ^2 and R again by solving simple quadratic equation.

In the case of nonzero ℓ^2 the boundary of the image of the $\mathcal{EM}$ map is defined by Eq. (A.26) in terms of (R,ℓ^2,x) variables and parameter u. This equation describes all the surface boundary. At the same time except simple (first order) touching points between energy level and boundary of the reduced phase space, there are also second order touching points where Eq. (A.26) has two degenerate roots and third order touching points where Eq. (A.26) has three coinciding roots. There are only isolated points of the third order touching and one-dimensional lines of points corresponding to second order touching.

A.3. Exceptional points of triple touching

We start by finding isolated points of the third order touching. In order to do that we use the fact that the equation of degree 5 with one triply degenerate root can be written in the form:

$$R^5+(-3t-s)R^4+(3t^2+3ts+p)R^3+(-t^3-3t^2s-3tp)R^2+(t^3s+3t^2p)R-t^3p=0. \quad (A.27)$$

In (A.27) we denote by t the triply degenerate root and by s and p the sum and product of two other roots. From the comparison of Eq. (A.27) with touching Eq. (A.26) we get the system of five equations by putting equality between corresponding coefficients of R-polynomials.

Then we eliminate consecutively variables s, p, ℓ^2 from this system of equations. Two resulting equations depend on variables t and x and on parameter u. One of the resulting equations is cubic in x, another is quartic in x. (Their degree in t is respectively 5 and 9.) In order to eliminate x we calculate the resultant of these two equations in x. (For applications of resultant to solving polynomial equations see, for example [33–35].) The so obtained resultant is a polynomial in t of degree 29 which can be factorized and written in a rather simple form

$$294912u^{18}t^5(t+2+2tu^6-2u^6+tu^{12})^2(t^2+t^2u^{12}+2t^2u^6+4t+4-4tu^6)^4 \times(-24tu^{12}-4+12t^2u^6-16u^6+12u^{12}+18t^2u^{12}-12tu^{18}-12tu^6 +3t^2u^{24}+12t^2u^{18}+3t^2)^4(tu^6+t-2)^6. \quad (A.28)$$

Each factor in resultant is maximally quadratic in t. All solutions can be easily found. The solution which we are interested in should go to 0 when u goes to 1. That solution for t is the solution for the value of R corresponding to third order touching point between energy level and the boundary of reduced phase space. We denote the corresponding point by A. For R_A we get

$$R_A=\frac{2(u^6-1)}{(1+u^6)^2}. \quad (A.29)$$

Author's personal copy

Now by substituting the so obtained R_A value into the polynomial equation resulting after eliminating s, p, ℓ^2 we obtain the corresponding x_A value and further consecutively ℓ_A^2, S_A, and E_A values, which are listed in Table 1.

A.4. Singular lines of double touching

In order to find singular lines which correspond to points of second order touching between energy level and the reduced phase space boundary we follow the same strategy as we used in the previous subsection for points of third order contact.

We use again Eq. (A.26) as a starting point. As soon as this equation is supposed to have one doubly degenerate root, it has the form

$$R^5+(-2t-s)R^4+(t^2+2ts+p_2)R^3+(-t^2s-2tp_2-p_3)R^2+(t^2p_2+2tp_3)R-t^2p_3=0, \tag{A.30}$$

where t is the doubly degenerate root, $s=t_3+t_4+t_5$ is the sum of three other roots which we denote by t_3, t_4, t_5, $p_2=t_3t_4+t_3t_5+t_4t_5$, and $p_3=t_3t_4t_5$. We get easily system of five equations from the equality of corresponding coefficients in R-polynomials (A.26) and (A.30). Eliminating consecutively from this system of equations s, p_2, p_3 we arrive at two polynomial equations depending on ℓ^2, x, t variables and parameter u. The so obtained equations are only quadratic in ℓ^2 and x but of degree 4 and 5 in t. Calculating resultants of these two equations with respect to ℓ^2 and x, we get two new polynomial equations. One depends on t, x, another on t, ℓ^2. In both cases polynomials can be decomposed in factors which are at most quadratic in x and in ℓ^2. This means that we can easily write down the explicit parametric representation for this curves in the form $(\ell^2(R;u), x(R;u))$. As soon as equations for x and for ℓ^2 are quadratic in R we have two solutions and the physically interesting for us now is the solution which goes to zero as $R\to 0$. We denote the corresponding solution as x_2 and ℓ_2^2 in order to indicate that these solutions correspond to second order touching points and represent them in the following form:

$$\begin{aligned} x_2=\frac{1}{16u^6}\Big(&-(u^6+1)^4R^3+6(u^6-1)(u^6+1)^2R^2-12(u^6-1)^2R-8(u^6+1)\\ &+(u^6+1)\left[4+4(1-u^6)R+(u^6+1)^2R^2\right]^{3/2}\Big), \end{aligned} \tag{A.31}$$

$$\begin{aligned} \ell_2^2=\frac{1}{4u^6}\Big(&-(u^6-1)(u^6+1)^2R^3+6(u^{12}+1)R^2-12(u^6-1)R+8\\ &-\left[4+4(1-u^6)R+(u^6+1)^2R^2\right]^{3/2}\Big), \end{aligned} \tag{A.32}$$

From (A.31, A.32) we recalculate immediately the corresponding S and E values.

$$\begin{aligned} E_2=\frac{1}{8u^6}\Big(&(u^6+1)^3R^3+6(u^6+1)R^2-12(u^6-1)R+8\\ &-\left[4+4(1-u^6)R+(u^6+1)^2R^2\right]^{3/2}\Big); \end{aligned} \tag{A.33}$$

$$\begin{aligned} S_2=\frac{1}{8u^6}\Big(&(u^6+1)^3R^3+2R^2(3+2u^6-u^{12})+4R(3-u^6)\\ &+8-\left[4+4(1-u^6)R+(u^6+1)^2R^2\right]^{3/2}\Big). \end{aligned} \tag{A.34}$$

Author's personal copy

It is easy to verify that by substituting into ((A.31)–(A.34)) values of R corresponding to points 0, A, B we get, respectively, values of x, ℓ^2, E, S in corresponding points. These values are given in Table 1.

Let us note that expressions for x_2, ℓ_2^2, E_2 have polynomial in R part and the square root part. The expression under the square root is the same in all formulae. This means that we can construct two linearly independent combinations of x_2, ℓ_2^2, E_2 which do not include square root and are completely polynomial. For example, we can take

$$4E_2 - 2\ell_2^2 = R^2\Big(R(1+u^6)^2 + 3(1-u^6)\Big), \tag{A.35}$$

$$4E_2(1+u^6) + 8x_2 = 3R\Big(R(1+u^6)^2 + 4(1-u^6)\Big). \tag{A.36}$$

A.5. 2D boundary of the image of $\mathcal{EM}$ map

In order to construct the 2D-boundary of the image of $\mathcal{EM}$ map we need to represent the equation of the boundary in a suitable parametric form. To get such representation from three initial equations describing respectively energy level, reduced phase space boundary and touching condition:

$$E = S - R + \frac{u^6+1}{4}R^2; \tag{A.37}$$

$$S^2 = (R^2 - \ell^2)(1 + x - R), \tag{A.38}$$

$$S(-2 + R(1+u^6)) + 2R + 2Rx - 3R^2 + \ell^2 = 0, \tag{A.39}$$

we eliminate S from (A.37–A.39) and get the system of two equations depending on R, x, ℓ^2, E and parameter u.

$$(R^2 - \ell^2)(1 + x - R) - \left(R - \frac{1}{4}R^2(1+u^6) + E\right)^2 = 0, \tag{A.40}$$

$$\left(R - \frac{1}{4}R^2(1+u^6) + E\right)\big(-2 + R(1+u^6)\big) + 2R + 2Rx - 3R^2 + \ell^2 = 0. \tag{A.41}$$

Now by eliminating from (A.40,A.41) either E or x (we calculate respectively resultant with respect to E or x variable) we get one equation depending on x, ℓ^2, R variables and another equation depending on E, ℓ^2, R variables. As soon as the first equation is quadratic in x and the second is quadratic in E, we easily get parametric representation of the boundary surface in the form $(E(R,\ell^2), x(R,\ell^2))$.

$$E_b = \frac{1}{4R}\Big(\ell^2 R(1+u^6) - 2(R^2+\ell^2) + (R^2-\ell^2)\sqrt{4 + 4R(1-u^6) + R^2(1+u^6)^2}\Big), \tag{A.42}$$

$$x_b = \frac{1}{8R^2}\Big(R^4(1+u^6)^2 + 4R^3(2-u^6) - R^2[\ell^2(1+u^6)^2 + 4] + 4R\ell^2u^6 - 4\ell^2 + (R^2-\ell^2)(2 - R(1+u^6))\sqrt{R^2(1+u^6)^2 + 4R(1-u^6) + 4}\Big). \tag{A.43}$$

Author's personal copy

Using this parametric representation we construct the 3D view of the boundary surface as shown in Fig. 15.

A.6. Lines of self-intersection

We now proceed to the analytic description of the line of self-intersection of the boundary of the image of $\mathcal{EM}$ map. We write the system of equations valid only for the points lying on the self-intersection line of the boundary. As soon as all points on the boundary are represented in (A.42,A.43) in parametric $(E_b(R,\ell^2), x_b(R,\ell^2))$ form with R and ℓ^2 as parameters the points on the line of self-intersection are characterized by the fact that the same point in E, x, ℓ^2 space can be obtained with two different values of parameters. So, we need to find such R_1 and R_2 values that

$$E_b(R_1) = E_b(R_2), \tag{A.44}$$

$$x_b(R_1) = x_b(R_2). \tag{A.45}$$

Eqs. (A.44, A.45) depend on R_1, R_2 and ℓ^2. General idea is to eliminate ℓ^2 and to get the equation describing the relation between R_1 and R_2. From the technical point of view it is simpler initially to introduce auxiliary variable Z_R which is related with R by simple quadratic equation

$$Z_R^2 = R^2(1+u^6)^2 + 4R(1-u^6) + 4. \tag{A.46}$$

Z_R is in fact the essential R-dependent part of the discriminant of the quadratic Eqs. (A.40,A.41). After introducing $Z_R(R_1)$ and $Z_R(R_2)$ we get the system of polynomial equations.

Eliminating ℓ^2 from polynomial Eqs. (A.44, A.45) by calculating their resultant we get the polynomial equation relating R_1, R_2, $Z_R(R_1)$, $Z_R(R_2)$ which together with (A.46) enable us to eliminate $Z_R(R_1)$ and $Z_R(R_2)$ by calculating consecutively two resultants. The final resultant which gives the relation between R_1 and R_2 has especially nice form

$$256(R_1-R_2)^6\Big(R_1(1+u^6)^2 + R_2(1+u^6)^2 + 4(1-u^6)\Big)^2 = 0. \tag{A.47}$$

This means that the relation between R_1 and R_2 is linear

$$R_1 + R_2 = \frac{4(u^6-1)}{(1+u^6)^2}. \tag{A.48}$$

It is easy to verify that for the point A the both values of R coincide $R_1 = R_2 = 2(u^6-1)/(1+u^6)^2$ whereas for point C the two values of R are 0 and $4(u^6-1)/(1+u^6)^2$. This means that in order to find all points on the self-intersection line we need to vary R between $2(u^6-1)/(1+u^6)^2$ and $4(u^6-1)/(1+u^6)^2$ or equivalently between 0 and $2(u^6-1)/(1+u^6)^2$.

The next step is to use the so found relation between R_1 and R_2 and to show that for these values of R we have $Z_R(R_1) = Z_R(R_2)$. Putting these relations into (A.44) gives us the expression of ℓ^2 as a function of R and Z_R for points on the self-intersection line.

$$(\ell^2)_{s-i} = \frac{R(Z_R-2)\Big(R(u^6+1)^2 + 4(1-u^6)\Big)}{(u^6+1)^2(Z_R+2)}. \tag{A.49}$$

Author's personal copy

In (A.49) the Z_R stands for positive solution of (A.46). Now by putting (A.49) into equation of the energy of the boundary points (A.42) we get the explicit expression for the energy of points on the self-intersection line.

$$E_{s-i} = \frac{R(Z_R(1+u^6) - 2(3-u^6))\left(R(u^6+1)^2 + 4(1-u^6)\right)}{4(u^6+1)^2(Z_R+2)}. \tag{A.50}$$

In a similar way we get the expression for the x coordinates of points on the self-intersection line.

$$X_{s-i} = \frac{R^2(u^6+1)^3 + 4R(1-u^{12}) - 2 + 4u^6 - Z_R(1-u^6)^2}{(u^6+1)^2(Z_R+2)}. \tag{A.51}$$

Finally expressions ((A.49)–(A.51)) give the representation of the self-intersection line as a function of R. The parameter R should vary either between 0 and $2(u^6-1)/(1+u^6)^2$ or between $2(u^6-1)/(1+u^6)^2$ and $4(u^6-1)/(1+u^6)^2$ in order to cover once all points on the self-intersection line.

We can also represent points on the self-intersection line in an alternative way expressing ℓ^2,E,x as a functions of Z_R.

$$(\ell^2)_{s-i} = \frac{(Z_R-2)^2}{(1+u^6)^2}, \tag{A.52}$$

$$E_{s-i} = \frac{(Z_R-2)(Z_R(1+u^6)+2u^6-6)}{4(u^6+1)^2}, \tag{A.53}$$

$$X_{s-i} = -\frac{3+u^{12}-Z_R(1+u^6)}{(u^6+1)^2}. \tag{A.54}$$

Moreover for all self-intersection points we can express their ℓ^2 and E coordinates explicitly as functions of x.

$$(\ell^2)_{s-i} = \left(\frac{(1-u^6)^2}{(1+u^6)^2} + x\right)^2, \tag{A.55}$$

$$E_{s-i} = x^2\frac{(1+u^6)}{4} + x\frac{(u^6-1)}{2} + \frac{(u^6+3)(u^6-1)^3}{4(u^6+1)^3}. \tag{A.56}$$

In (A.55) and (A.56) x varies between its values for x_A and x_C points $x_A \leqslant x \leqslant x_C$ (see Table 1).

References

[1] P. Lynch, Intl. J. Nonlin. Mech. 37 (2002) 345–367;
P. Lynch, C. Houghton, Physica D 190 (2004) 38–62.
[2] D.D. Holm, P. Lynch, SIAM J. Applied Dyn. Syst. 1 (2002) 44–64.
[3] H. Dullin, A. Giacobbe, R.H. Cushman, Physica D 190 (2004) 15–37.
[4] A. Giacobbe, R.H. Cushman, D.A. Sadovskií, B.I. Zhilinskií, J. Math. Phys. 45 (12) (2004) 5076–5100.
[5] J.J. Duistermaat, Comm. Pure Appl. Math. 33 (1980) 687–706.
[6] L.M. Bates, R.H. Cushman, Global Aspects of Classical Integrable Systems, Birkhäuser, Basel, 1997.
[7] S. Vũ Ngọc, Comm. Math. Phys. 203 (1999) 465–479.
[8] R.H. Cushman, J.J. Duistermaat, Bull. Am. Math. Soc. 19 (1988) 475–479.

Author's personal copy

[9] B.I. Zhilinskii, in: M. Monastyrsky (Ed.), Topology in Condensed Matter, vol. 150, Springer Series in Solid State Sciences, 2006, pp. 165–186.
[10] R.H. Cushman, H.R. Dullin, A. Giacobbe, D.D. Holm, M. Joyeux, P. Lynch, D.A. Sadovskií, B.I. Zhilinskií, Phys. Rev. Lett. 93 (2004) 024302-1–024302-4.
[11] M. Sanrey, M. Joyeux, D. Sadovskii, J. Chem. Phys. 124 (2006) 074318-1–074318-12.
[12] C.D. Cooper, M.S. Child, Phys. Chem. Chem. Phys. 7 (2005) 2731–2739, Figs. 7 and 8 of this paper are corrected in [13].
[13] M. Child, Adv. Chem. Phys. (in press).
[14] J.C. van der Meer, The Hamiltonian Hopf Bifurcation, Ser. Lect. Notes Math., vol. 1160, Springer, Berlin, 1985.
[15] R.H. Cushman, J.C. van der Meer, Lect. Notes Math. 1416 (1991) 26–38.
[16] D.A. Sadovskií, R.H. Cushman, Physica D 142 (2000) 166–196.
[17] H. Hanßmann, J.C. van der Meer, J. Dyn. Diff. Eq. 14 (2002) 675–695.
[18] K. Efstathiou, D.A. Sadovskií, R.H. Cushman, Proc. Roy. Soc. (London) Ser. A 459 (2040) (2003) 2997–3019.
[19] K. Efstathiou, D.A. Sadovskií, Nonlinearity 17 (2) (2004) 415–446.
[20] K. Efstathiou, R.H. Cushman, D.A. Sadovskií, Physica D 194 (2004) 250–274.
[21] H. Waalkens, A. Junge, H.R. Dullin, J. Phys. A. Math. Gen. 36 (2003) L307–L314.
[22] H. Waalkens, P.H. Richter, H.R. Dullin, Physica D 196 (2004) 265–310.
[23] K. Efstathiou, Metamorphoses of Hamiltonian systems with symmetries, Ser. Lect. Notes Math., vol. 1864, Springer, Berlin, 2004.
[24] N.N. Nekhoroshev, D.A. Sadovskií, B.I. Zhilinskií, Ann. Henri Poincaré, 7 (2006) 1099–1211.
[25] M. Joyeux, D.A. Sadovskií, J. Tennyson, Chem. Phys. Lett. 382 (3–4) (2003) 439–442.
[26] K. Efstathiou, M. Joyeux, D.A. Sadovskií, Phys. Rev. A 69 (2004) 032504-1–032504-15.
[27] M. Joyeux, S.C. Farantos, R. Schinke, J. Phys. Chem. A 106 (2002) 5407–5421.
[28] C. Zhou, D. Xie, R. Chen, G. Yan, H. Guo, V. Tyng, M. Kellman, Spectrochim. Acta A 58 (2002) 727–746.
[29] M. Joyeux, S.Yu. Grebenschikov, J. Bredendeck, R. Schinke, S. Farantos, Adv. Chem. Phys. 130 (Part A) (2005) 267–302.
[30] N.N. Nekhoroshev, D.A. Sadovskií, B.I. Zhilinskií, C. R. Acad. Sci. Paris, Ser. I 335 (2002) 985–988.
[31] D.A. Sadovskií, B.I. Zhilinskií, Mol. Phys. 104 (2006) 2595–2615.
[32] A.V. Bolsinov, A.T. Fomenko, Integrable Hamiltonian Systems. Geometry, Topology, Classification, Chapman & Hall/CRC, London/Boca Raton, FL, 2004.
[33] W.V.D. Hodge, D. Pedoe, Methods of Algebraic Geometry, vol. 1, Cambridge University Press, Cambridge, 1953.
[34] D. Cox, J. Little, D. O'Shea, Using Algebraic geometry, Springer, New York, 1998.
[35] B. Sturmfels, Solving Systems of Polynomial Equations, University of California, AMS, 2002.
[36] D. Sugny, H. Jauslin, M. Joyeux, (unpublished).
[37] A. Giacobbe, (unpublished).

Author's personal copy